SFB/CPP-10-34
TTP/10-23
HU-EP-10/25
WUB/10-13

# Light MSSM Higgs boson mass to three-loop accuracy

P. Kant[(a)], R.V. Harlander[(b)], L. Mihaila[(c)], M. Steinhauser[(c)]

*(a) Institut für Physik, Humboldt-Universität zu Berlin*
*12489 Berlin, Germany*
*(b) Fachbereich C, Theoretische Physik, Universität Wuppertal*
*42097 Wuppertal, Germany*
*(c) Institut für Theoretische Teilchenphysik, Karlsruhe Institute of Technology (KIT)*
*76128 Karlsruhe, Germany*

**Abstract**

The light CP even Higgs boson mass, $M_h$, is calculated to three-loop accuracy within the Minimal Supersymmetric Standard Model (MSSM). The result is expressed in terms of $\overline{\rm DR}$ parameters and implemented in the computer program `H3m`. The calculation is based on the proper approximations and their combination in various regions of the parameter space. The three-loop effects to $M_h$ are typically of the order of a few hundred MeV and opposite in sign to the two-loop corrections. The remaining theory uncertainty due to higher order perturbative corrections is estimated to be less than 1 GeV.

PACS numbers: 12.60.Jv, 14.80.Da, 12.38.Bx

# 1 Introduction

Among the main expectations in view of the CERN Large Hadron Collider (LHC) is to provide clear phenomena beyond the Standard Model (SM) of particle physics. A very promising candidate for an extension of the SM is the so-called Minimal Supersymmetric Standard Model (MSSM) which relies on an extended symmetry between fermions and bosons [1, 2]. It is constructed in such a way that in the low-energy limit the SM is recovered thus leading to the same phenomena in the energy range around the electroweak scale. In particular, the MSSM is in accordance with the electroweak precision data [3]. At the same time it provides a dark matter candidate, solves the hierarchy problem and provides a platform where also gravitational interactions can be included.

An appealing feature of the MSSM is the quite restrictive Higgs sector which is described at leading order by two independent parameters. In particular, the mass of the lightest CP-even Higgs boson, $M_h$, is not a free parameter, like in the SM, but a prediction which can be used in order to test this minimal supersymmetric extension of the SM.

$M_h$ is very sensitive to radiative corrections. In lowest order it is bound from above by the $Z$ boson mass which is already excluded by experiment. Already quite some time ago it has been observed that large one-loop corrections, in particular from the top quark and top squark sector can raise $M_h$ to about 140 GeV [4–6]. In the meantime a number of higher order corrections have been computed including even CP-violating couplings and improvements from renormalization group considerations (see Refs. [7–9] for a review). In this paper we consider neither CP violation nor the resummation of higher order logarithms. Let us nevertheless mention that in particular CP violating phases can lead to a shift of a few GeV in $M_h$, see, e.g., Refs. [**?**, **?**]. In Ref. [10] a large class of two-loop corrections to the lightest Higgs boson mass have been considered and in Ref. [11] leading logarithmic corrections at three-loop order have been computed. The first complete three-loop calculation of the leading quartic top quark mass terms within supersymmetric QCD (SQCD; more precisely, this means supersymmetric six-flavor QCD coupled to the MSSM Higgs sector) has been performed in Ref. [12] for a degenerate supersymmetric mass spectrum. It is the aim of this paper to provide details and extend this calculation.

At the moment there are two computer programs publicly available which include most of the higher order corrections. `FeynHiggs` has been available already since 1998 [13, 14, 9] and has been continuously improved since then [15, 16]. In particular, it contains all numerically important two-loop corrections and accepts both real and complex MSSM input parameters. The second program, `CPSuperH` [17, 18], is based on a renormalization group improved diagrammatic calculation and allows for explicit CP violation. Both programs compute the mass spectrum as well as the decay width of the neutral and charged Higgs bosons.

In this paper we discuss the three-loop corrections originating from the strong sector of the MSSM which are proportional to the quartic top quark mass. At three-loop order

several mass scales enter the Feynman diagrams making their evaluation quite involved. In addition to the top quark mass there are the top squark masses, the gluino mass and the masses of the remaining squarks. An exact evaluation of the three-loop integrals is currently out of range. However, it is possible to apply expansion techniques for various limits which allow to cover a large part of the supersymmetric (SUSY) parameter space. In particular, we can construct precise approximations for the Snowmass Points and Slopes (SPS) [19, 20]. Our set-up is easily extendable to other regions of parameter space which may become interesting in future.

Together with this paper we provide a `Mathematica` program, `H3m` [21], which contains all our three-loop results. Furthermore, `H3m` constitutes an interface to `FeynHiggs` [22] and various SUSY spectrum generators which allows for precise predictions of $M_h$ on the basis of realistic SUSY scenarios.

The remainder of the paper is organized as follows: In the next Section we revisit the two-loop corrections. In particular, we construct approximations which are also available at three-loop order and compare with the exact result. In Section 3 we provide details on our three-loop calculations for the various hierarchies. In particular we discuss the renormalization and the asymptotic expansion. Section 4 describes the implementation of our results in the computer program `H3m` and the phenomenological implementations are discussed in Section 5. We present a summary and the conclusions in Section 6. In the Appendices additional material is provided, in particular all the one- and two-loop counterterms that have entered in our calculation.

# 2 $M_h$ in the MSSM

## 2.1 Higgs boson sector of the MSSM

The mass of the Higgs boson is obtained from the quadratic terms in the corresponding potential which for the MSSM has the following form:

$$\begin{aligned} V_H = & \left(|\mu_{\rm SUSY}|^2 + m_1^2\right)|H_1|^2 + \left(|\mu_{\rm SUSY}|^2 + m_2^2\right)|H_2|^2 \\ & - m_{12}^2\left(\epsilon_{ab}H_1^a H_2^b + \epsilon_{ab}H_1^{a*}H_2^{b*}\right) \\ & + \frac{1}{8}\left(g_1^2+g_2^2\right)\left[|H_1|^2 - |H_2|^2\right]^2 + \frac{1}{2}g_2^2\left|H_1^\dagger H_2\right|^2 . \end{aligned} \tag{1}$$

with $\epsilon_{12} = -\epsilon_{21} = 1$ and $\epsilon_{11} = \epsilon_{22} = 0$. $\mu_{\rm SUSY}$ is the Higgs-Higgsino bilinear coupling from the super potential and $m_1, m_2$ and $m_{12}$ are soft breaking parameters. Note that the quartic terms are fixed by the SU(2) and U(1) gauge couplings $g_1$ and $g_2$. The parameters

in (1) are related to the masses of the gauge bosons and the pseudoscalar Higgs via

$$\begin{aligned} M_W^2 &= \frac{1}{2} g_2^2 \left(v_1^2 + v_2^2\right), \\ M_Z^2 &= \frac{1}{2} \left(g_1^2 + g_2^2\right) \left(v_1^2 + v_2^2\right), \\ M_A^2 &= -m_{12}^2 \left(\tan\beta + \cot\beta\right), \end{aligned} \tag{2}$$

where $\tan\beta = v_2/v_1$.

After spontaneous symmetry breaking the neutral components of the doublets $H_1$ and $H_2$ acquire the vacuum expectation values $v_1$ and $v_2$, and we write

$$\begin{aligned} H_1 &= \begin{pmatrix} v_1 + \frac{1}{\sqrt{2}} \left(\phi_1 + i\chi_1\right) \\ -\phi_1^- \end{pmatrix}, \\ H_2 &= \begin{pmatrix} \phi_2^+ \\ v_2 + \frac{1}{\sqrt{2}} \left(\phi_2 + i\chi_2\right) \end{pmatrix}, \end{aligned} \tag{3}$$

which leads to the following representation of the Higgs boson mass matrix at tree level:

$$\mathcal{M}_{H,\text{tree}}^2 \;=\; \frac{1}{2} \frac{\partial^2 V}{\partial\phi_1 \partial\phi_2} = \frac{\sin 2\beta}{2} \begin{pmatrix} M_Z^2 \cot\beta + M_A^2 \tan\beta & -M_Z^2 - M_A^2 \\ -M_Z^2 - M_A^2 & M_Z^2 \tan\beta + M_A^2 \cot\beta \end{pmatrix}, \tag{4}$$

where we restrict ourselves to the two CP-even Higgs bosons.

In this paper we restrict ourselves to the numerically dominant $m_t^4$ corrections. As a consequence we can set the electroweak gauge couplings to zero and furthermore nullify the external momentum in the occurring two-point functions. The formalism presented in the following is adapted to this framework.

It is convenient to evaluate the quantum corrections in the $\{\phi_1, \phi_2\}$ basis which requires the evaluation of self energy corrections $\Sigma_{\phi_1}$ and $\Sigma_{\phi_2}$ involving $\phi_1$ and $\phi_2$. Denoting renormalized quantities with a hat, Eq. (4) gets modified to

$$\mathcal{M}_H^2 \;=\; \mathcal{M}_{H,\text{tree}}^2 - \begin{pmatrix} \hat{\Sigma}_{\phi_1} & \hat{\Sigma}_{\phi_1\phi_2} \\ \hat{\Sigma}_{\phi_1\phi_2} & \hat{\Sigma}_{\phi_2} \end{pmatrix}, \tag{5}$$

with [15]

$$
\begin{aligned}
\hat{\Sigma}_{\phi_1} = \Sigma_{\phi_1} &- \Sigma_A \sin^2\beta \\
&+ \frac{e}{2M_W \sin\vartheta_W} t_{\phi_1} \cos\beta \left(1 + \sin^2\beta\right) \\
&- \frac{e}{2M_W \sin\vartheta_W} t_{\phi_2} \cos^2\beta \sin\beta \,, \\
\hat{\Sigma}_{\phi_2} = \Sigma_{\phi_2} &- \Sigma_A \cos^2\beta \\
&- \frac{e}{2M_W \sin\vartheta_W} t_{\phi_1} \sin^2\beta \cos\beta \\
&+ \frac{e}{2M_W \sin\vartheta_W} t_{\phi_2} \sin\beta \left(1 + \cos^2\beta\right) \,, \\
\hat{\Sigma}_{\phi_1\phi_2} = \Sigma_{\phi_1\phi_2} &+ \Sigma_A \sin\beta\cos\beta \\
&+ \frac{e}{2M_W \sin\vartheta_W} t_{\phi_1} \sin^3\beta \\
&+ \frac{e}{2M_W \sin\vartheta_W} t_{\phi_2} \cos^3\beta \,.
\end{aligned}
\tag{6}
$$

In this equation, $\vartheta_W$ is the weak mixing angle, $\Sigma_A$ denotes the self energy of the pseudoscalar Higgs boson and $t_{\phi_i}$ the tadpole contributions of the field $\phi_i$. Typical diagrams to the individual contributions can be found in Fig. 1. Since we are only interested in the leading corrections proportional to $m_t^4$ we evaluate the quantum corrections in the limit of vanishing external momentum [23–25].

For the evaluation of the lightest Higgs boson mass we consider in a first step the matrix element of $\mathcal{M}_H^2$ to a given order in perturbation theory. Subsequently, we determine the eigenvalues and assign the smaller one to $M_h$. We perform this procedure at tree level and at one-, two-, and three-loop order which leads to the corresponding approximations of the Higgs boson mass. It is convenient to introduce the quantity

$$
\Delta M_h^{(i)} \;=\; M_h^{(i-\text{loop})} - M_h^{\text{tree}} \,, \tag{7}
$$

representing the difference between the Higgs boson mass evaluated with $i$-loop accuracy and the tree-level result.

## 2.2 Top squark sector of the MSSM

In this paper we only consider strong corrections which means that apart from the quarks and gluons also the corresponding superpartners, the squarks and gluinos, are present. The leading contribution proportional to $G_F m_t^4$ is generated by the top quark Yukawa coupling which distinguishes the top squark sector from the other squark parts of the MSSM Lagrange density. In order to fix the notation let us discuss in more detail the mass matrix of the left- and right-handed component of the top squark, $\tilde{t}_L$ and $\tilde{t}_R$, which

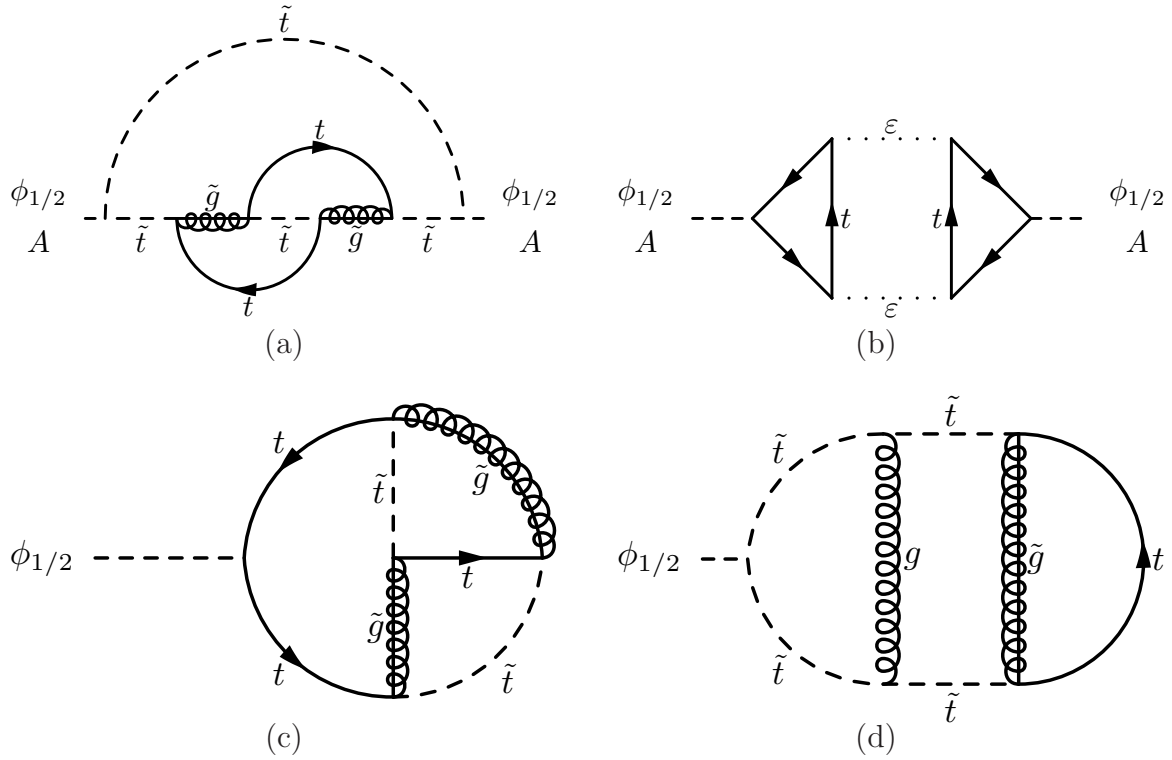


Figure 1: Sample diagrams contributing to $\Sigma_{\phi_1}$, $\Sigma_{\phi_2}$, $\Sigma_{\phi_1\phi_2}$, $\Sigma_A$, $t_{\phi_1}$ and $t_{\phi_2}$. Internal solid, dashed, dotted and curly lines correspond to top quarks, top squarks, $\varepsilon$-scalar and gluons, respectively. Gluinos are depicted with as curly lines with an additional solid line in the middle. The external dashed line corresponds to the Higgs boson.

is given by

$$\begin{aligned}\mathcal{M}^2_{\tilde{t}} &= \begin{pmatrix} m_t^2 + M_Z^2\left(\frac{1}{2} - \frac{2}{3}\sin^2\vartheta_W\right)\cos 2\beta + M^2_{\tilde{Q}} & m_t\left(A_t - \mu_{\rm SUSY}\cot\beta\right) \\ m_t\left(A_t - \mu_{\rm SUSY}\cot\beta\right) & m_t^2 + \frac{2}{3}M_Z^2\sin^2\vartheta_W\cos 2\beta + M^2_{\tilde{U}} \end{pmatrix} \\ &\equiv \begin{pmatrix} m^2_{\tilde{t}_L} & m_t X_t \\ m_t X_t & m^2_{\tilde{t}_R} \end{pmatrix}, \end{aligned} \tag{8}$$

with $X_t = A_t - \mu_{\rm SUSY}\cot\beta$. $M_{\tilde{Q}}$ and $M_{\tilde{U}}$ are soft SUSY breaking masses, and $A_t$ is the soft SUSY breaking tri-linear coupling between the Higgs boson and the top squark fields.

Diagonalization of Eq. (8) leads to the mass eigenstates $\tilde{t}_1$ and $\tilde{t}_2$ with masses

$$m^2_{\tilde{t}_{1,2}} = \frac{1}{2}\left(m^2_{\tilde{t}_L} + m^2_{\tilde{t}_R} \mp \sqrt{\left(m^2_{\tilde{t}_L} - m^2_{\tilde{t}_R}\right)^2 + 4m_t^2 X_t^2}\right). \tag{9}$$

The mixing angle is defined through the unitary transformation

$$\begin{pmatrix} m^2_{\tilde{t}_1} & 0 \\ 0 & m^2_{\tilde{t}_2} \end{pmatrix} = \mathcal{R}^\dagger_{\tilde{t}}\mathcal{M}_{\tilde{t}}\mathcal{R}_{\tilde{t}}\,, \quad \text{with} \quad \mathcal{R}_{\tilde{t}} = \begin{pmatrix} \cos\theta_t & -\sin\theta_t \\ \sin\theta_t & \cos\theta_t \end{pmatrix}, \tag{10}$$

and

$$\sin 2\theta_t = \frac{2m_t(A_t - \mu_{\rm SUSY}\cot\beta)}{m^2_{\tilde{t}_1} - m^2_{\tilde{t}_2}}\,. \tag{11}$$

## 2.3 Leading $m_t^4$ corrections in the on-shell and $\overline{\rm DR}$ scheme

As already mentioned above, the numerically dominant contribution arises from the self energy diagrams evaluated for vanishing external momentum. Thus, it is convenient to introduce the following notation for the $i$-loop corrections to the Higgs boson mass

$$\Delta M_h^{(i)} \;=\; \Delta^{m_t^4} M_h^{(i)} + \Delta^{\rm rem} M_h^{(i)}\,, \tag{12}$$

where $\Delta^{m_t^4} M_h^{(i)}$ comprises the complete SQCD contribution of order $\alpha_t\alpha_s^{i-1}$ ($\alpha_t$ is the top Yukawa coupling) originating from the top quark/squark sector for vanishing external momentum which is proportional to $m_t^4$. At one-loop order only top quarks and top squarks are present in the loops. The two- and three-loop corrections, $\Delta^{m_t^4} M_h^{(2)}$ and $\Delta^{m_t^4} M_h^{(3)}$, are obtained by adding gluon, gluino, quark and squark contributions. $\Delta^{\rm rem} M_h^{(i)}$ represents the remaining part which is only available at one- and two-loop order. In our approach these corrections are taken from `FeynHiggs` which includes the complete one-loop corrections and all available two-loop terms.[1] At three-loop order only the contribution $\Delta^{m_t^4} M_h^{(3)}$ is considered.

In the following we discuss the relative contribution to the Higgs boson mass comparing $\Delta M_h^{(i)}$ and $\Delta^{m_t^4} M_h^{(i)}$ at one- and two-loop order ($i = 1, 2$) where both the on-shell and $\overline{\rm DR}$ scheme for the mass parameters and the mixing angle are considered. For illustration we adopt the scenarios SPS1a and SPS2 and show the Higgs boson mass as a function of $m_{1/2}$.

The solid lines in Fig. 2 show the results for $\Delta M_h^{(i)}$ using on-shell parameters[2] for the masses and $\theta_t$ as it is provided by `FeynHiggs`. The dashed lines correspond to the $m_t^4$ approximation ($\Delta^{m_t^4} M_h^{(i)}$) which can be found in Refs. [15, 26] and has been confirmed by us by an independent calculation. The panels (a) and (b) correspond to the SPS1a and SPS2 benchmark scenarios, respectively, where the input parameters have been generated with the help of `SOFTSUSY` [27]. The small differences of the solid and dashed lines[3] demonstrate that the leading top quark mass term approximates the full result to a high accuracy. This statement is also true in the $\overline{\rm DR}$ scheme. The corresponding two-loop results are shown in Fig. 2 as dash-dotted and dotted curves where the former corresponds to the full and the latter to the approximate result.

It is well known that the perturbative series can exhibit a bad convergence behaviour in

[1] For a detailed description we refer to the `FeynHiggs` home page [22].

[2] For the on-shell renormalization of the mixing angle we adopt the convention of Ref. [26].

[3] In the case of SPS1a the two-loop dashed line is almost on top of the solid one.

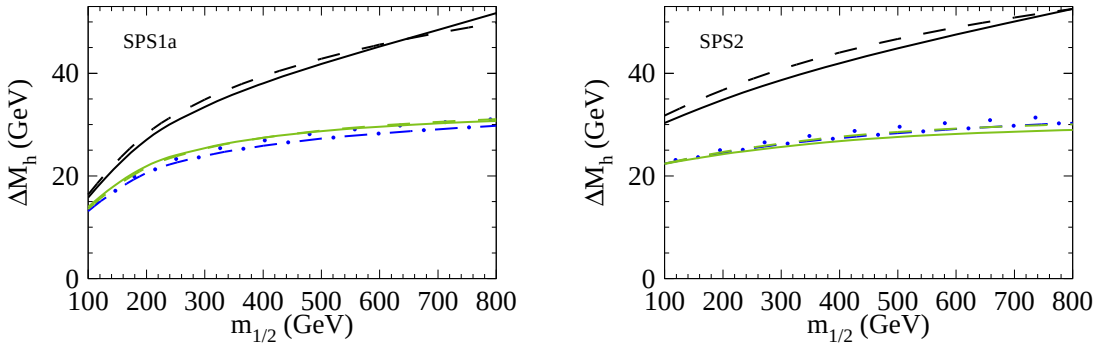


(a) (b)

Figure 2: Comparison of complete and approximate one- and two-loop corrections to the Higgs boson mass for SPS1a (a) and SPS2 (b). The solid (full result) and dashed lines ($m_t^4$ approximation) represent the results in the on-shell scheme where the upper and lower curves correspond to the one- and two-loop results, respectively. The two-loop $\overline{\rm DR}$ results are shown as dash-dotted (full result) and dotted ($m_t^4$ approximation) curves.

case it is parametrized in terms of the on-shell quark masses[4] which is due to intrinsically large contributions related to the infra-red behaviour of the theory. Thus, it is tempting to re-parametrize the results for the Higgs boson mass in terms of $\overline{\rm DR}$ parameters for the top quark mass, the masses of the SUSY particles and the top squark mixing angle. Since the corrections are dominated by $\Delta^{m_t^4} M_h^{(i)}$ it is sufficient to consider only this term and take over $\Delta^{\rm rem} M_h^{(i)}$ from the output of `FeynHiggs`. In the remainder of the paper we will refer to this renormalization scheme as $\overline{\rm DR}$ scheme although it contains a mixture of on-shell and $\overline{\rm DR}$ parameters. Let us mention already at this point that from outside this mixture does not pose any complication in the practical use since the spectrum generator produces both on-shell and $\overline{\rm DR}$ parameters which then serve as input for the evaluation of $M_h$.

Further below we will discuss the scheme dependence of $M_h$ and indeed show that the loop corrections are in general smaller in the $\overline{\rm DR}$ scheme (cf. Fig. 8). Similar studies can also be found in the literature [14, 8].

The considerations of this subsection motivates the following procedure at three loops: It is certainly sufficient to consider only the approximation $\Delta^{m_t^4} M_h^{(3)}$ since the size of the remaining term is expected to be below 100 MeV. Furthermore, we adopt the $\overline{\rm DR}$ scheme since we expect that the perturbative series shows a better convergence behaviour. In addition the evaluation of the counterterms themselves is significantly simpler. Actually, most of them are already available in the literature and the computation of the remaining ones is quite straightforward as we discuss in Appendix A. We provide the analytical

[4]For a typical example we refer to the electroweak $\rho$ parameter. Using the on-shell top quark mass the four-loop corrections [28–30] are larger by a factor 50 as compared to the $\overline{\rm MS}$ scheme.

results for the two-loop renormalization constants of the top squark masses and mixing angle, that can be easily expanded for the mass hierarchies considered in this paper. The multiplicative $\overline{\rm DR}$ renormalization constants of the top quark and gluino mass are mass independent and therefore valid for all hierarchies.

## 2.4 Construction of approximations

Considering the many different mass parameters entering the formula for the Higgs boson mass an exact calculation of the three-loop corrections is currently not feasible. However, due to the various hierarchies among the particle masses it is promising to consider expansions in properly chosen small parameters. As a guideline for the latter we follow the SPS scenarios as defined in Refs. [19, 20].

In order to construct approximations covering all SPS cases it is sufficient to consider the following hierarchies among the SUSY masses[5]

$$\begin{aligned}
&\text{(h3)} && m_{\tilde{q}} \approx m_{\tilde{t}_1} \approx m_{\tilde{t}_2} \approx m_{\tilde{g}}\,, \\
&\text{(h4)} && m_{\tilde{q}} \gg m_{\tilde{t}_1} \approx m_{\tilde{t}_2} \approx m_{\tilde{g}}\,, \\
&\text{(h5)} && m_{\tilde{q}} \gg m_{\tilde{t}_2} \gg m_{\tilde{t}_1} \approx m_{\tilde{g}}\,, \\
&\text{(h6)} && m_{\tilde{q}} \gg m_{\tilde{t}_2} \approx m_{\tilde{g}} \gg m_{\tilde{t}_1}\,, \\
&\text{(h6b)} && m_{\tilde{q}} \approx m_{\tilde{t}_2} \approx m_{\tilde{g}} \gg m_{\tilde{t}_1}\,, \\
&\text{(h9)} && m_{\tilde{q}} \approx m_{\tilde{t}_1} \approx m_{\tilde{t}_2} \gg m_{\tilde{g}}\,,
\end{aligned} \tag{13}$$

where in the case of "$\gg$" an asymptotic expansion in the corresponding hierarchy is performed. In the case of "$\approx$" a naive Taylor expansion in the difference of the particle masses is sufficient. Throughout this paper, $\tilde{q}$ denotes any squark other than $\tilde{t}$, and we assume a common mass value $m_{\tilde{q}} \equiv m_{\tilde{q}_1} = m_{\tilde{q}_2}$ for all of these "heavy squarks".

In all hierarchies we assume that the SUSY masses are larger than the top quark mass and perform an asymptotic expansion in the corresponding ratio. In the numerical results discussed below we include for the various hierarchies the expansion terms as given in

[5] We decided to keep the nomenclature for the hierarchies as they are in our internal computations and documents. The non-continuous numeration results from the fact that for testing purposes we have computed further hierachies which, however, are not included in the program `H3m` (cf. Section 4).

| hierarchy | expansion depth | | |
|---|---|---|---|
| (h3) | $(1-x_{12}^2)^3$, | $(1-x_{1g})^3$, | $(1-x_{1q}^2)^3$ |
| (h4) | | | $x_{1q}^8$ |
| (h5) | $(1-x_{1g})^2$, | $(x_{12})^4$, | $x_{2q}^4$ |
| (h6) | $x_{12}^3$, | $(1-x_{2g})^2$, | $x_{2q}^4$ |
| (h6b) | $x_{12}^3$, | $(1-x_{2g})^2$, | $(1-x_{2q}^2)^2$ |
| (h9) | $(1-x_{12}^2)^3$, | $1/x_{12}^4$, | $(1-x_{1q}^2)^3$ |

Table 1: Expansion terms available for the individual hierarchies as defined in Eq. (13) at three-loop order.

Tab. 1 where the following notation has been introduced

$$\begin{aligned} x_{12} &= \frac{m_{\tilde{t}_1}}{m_{\tilde{t}_2}}\,, \\ x_{2g} &= \frac{m_{\tilde{t}_2}}{m_{\tilde{g}}}\,, \\ x_{1g} &= x_{12}x_{2g} = \frac{m_{\tilde{t}_1}}{m_{\tilde{g}}}\,, \\ x_{1q} &= \frac{m_{\tilde{t}_1}}{m_{\tilde{q}}}\,, \\ x_{2q} &= \frac{m_{\tilde{t}_2}}{m_{\tilde{q}}}\,. \end{aligned} \tag{14}$$

Note that at two-loop order the contributions involving the squarks $\tilde{q}$ with $q \in \{u, d, s, c, b\}$ cancel in the sum of all diagrams. At three-loop level, however, the results depend on $m_{\tilde{q}}$. In those cases where $m_{\tilde{q}}$ is much larger than the other masses at least three expansion terms are computed and a good convergence even up to $m_{\tilde{q}} \approx m_{\tilde{t}_2}$ is observed.

In order to demonstrate this point we consider the hierarchies (h3) and (h4) and show in Fig. 3 the three-loop prediction for $M_h$. The dashed and solid lines correspond to (h4) including successively higher orders in $1/m_{\tilde{q}}$ where for illustration the following input parameters have been chosen:[6]

$$\begin{aligned} m_{\rm SUSY} &\equiv m_{\tilde{g}} = m_{\tilde{t}_1} = m_{\tilde{t}_2} = 800\,\text{GeV}\,, \\ A_t &= \mu_{\rm SUSY} = \theta_t = 0\,, \\ M_A &= 1500\ \text{GeV}\,. \end{aligned} \tag{15}$$

The horizontal ($m_{\tilde{q}}$-independent) dotted line corresponds to the scenario (h3) with $m_{\tilde{q}} = m_{\rm SUSY}$ fixed at 800 GeV. One observes a crossing of the latter and the (h4)-curve including $1/m_{\tilde{q}}^8$ corrections for $m_{\tilde{q}} \approx m_{\rm SUSY}$ which nicely demonstrates the rapid convergence in the

[6]If not stated otherwise we set the renormalization scale equal to the on-shell top quark mass and evaluate all $\overline{\rm DR}$ parameters at that scale. Note, however, that `H3m` is not restricted to this choice.

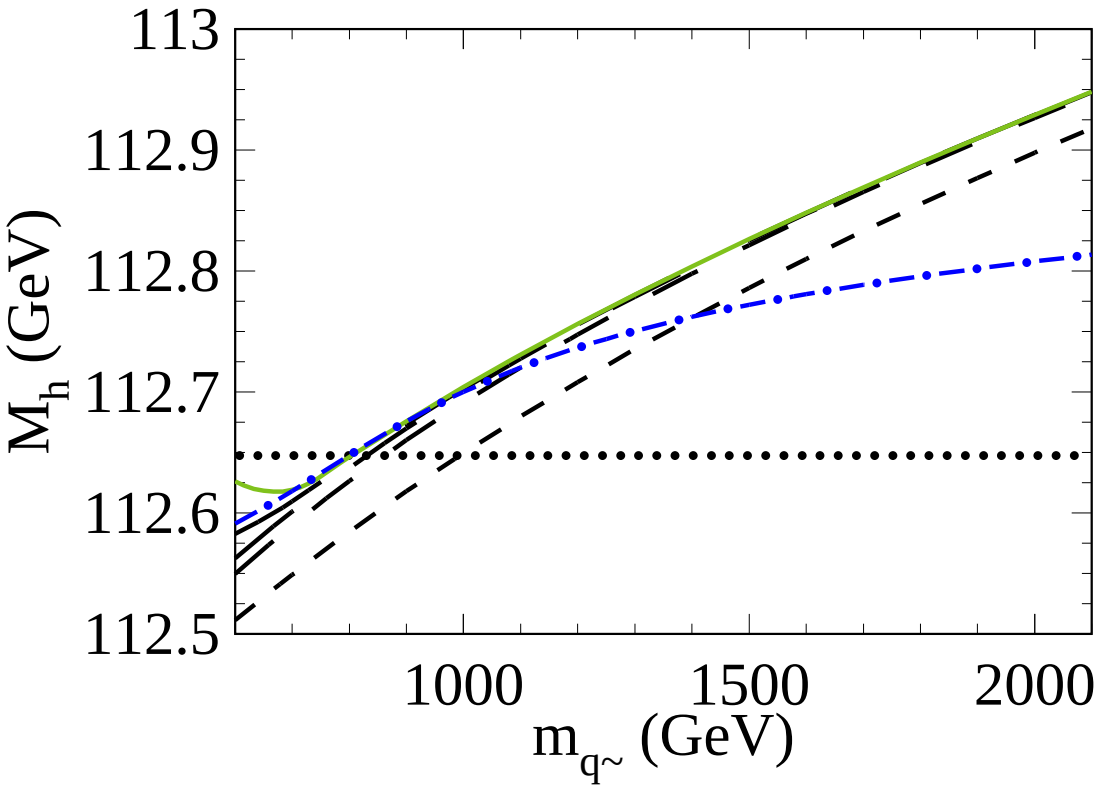


Figure 3: Dependence of the three-loop corrections on the heavy squark mass $m_{\tilde{q}}$. The dashed and solid lines correspond to the hierarchy (h4) where successively higher order terms in $m_{\rm SUSY}/m_{\tilde{q}}$ have been included (The solid curve contains terms of order $(m^2_{\rm SUSY}/m^2_{\tilde{q}})^4$.). The dotted and dash-dotted curves correspond to the hierarchy (h3); for the dotted line $m_{\tilde{q}}$ has been kept fixed at 800 GeV, the dash-dotted curve includes terms of order $(1 - m^2_{\rm SUSY}/m^2_{\tilde{q}})^3$.

large-$m_{\tilde{q}}$ expansion. Fig. 3 also shows that the expansion around $m_{\tilde{q}} = m_{\rm SUSY}$ leads to good approximations even if $m_{\tilde{q}}$ is two to three times as big as $m_{\rm SUSY}$, see dash-dotted curve. Note that for this plot we computed the $\overline{\rm DR}$ top quark mass for $m_{\tilde{q}} = 800$ GeV and kept it fixed.

Let us in a next step compare the approximate SQCD corrections according to our hierarchies with the full prediction for $M_h$ from Ref. [26]. For illustration we adopt in the remainder of this Section a minimal supergravity (MSUGRA) scenario with

$$\begin{aligned} \tan\beta &= 10\,, \\ A_0 &= 0\,, \\ \mu_{\rm SUSY} &> 0\,, \end{aligned} \tag{16}$$

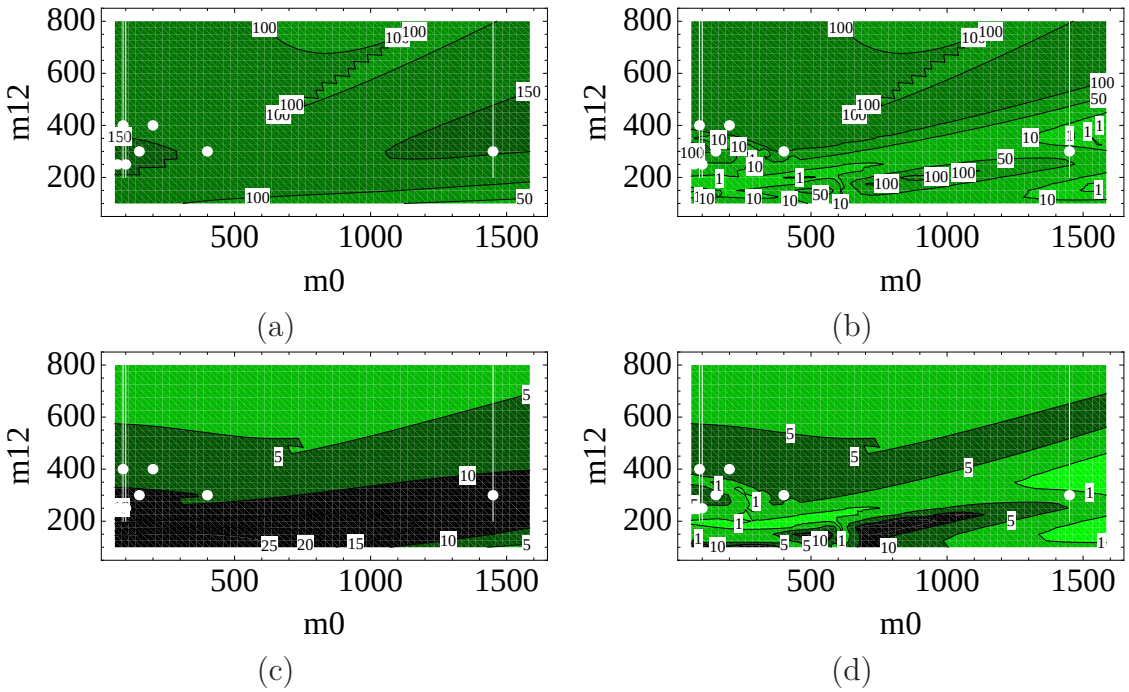


Figure 4: Comparison of approximate and full two-loop result for hierarchy (h3) (a) and the combination of (h3), (h5), (h6), (h6b) and (h9) (b). The contour lines indicate the deviations in MeV. In (c) and (d) the results of (a) and (b) are normalized to the genuine two-loop contributions where the contour lines indicate the deviations in per cent. The benchmark points and slopes are shown as (white) dots and lines.

and vary $m_0$ and $m_{1/2}$ as follows

$$\begin{aligned} 60 \text{ GeV} \quad &< m_0 < \quad 1600 \text{ GeV}\,, \\ 100 \text{ GeV} \quad &< m_{1/2} < \quad 800 \text{ GeV}\,. \end{aligned} \tag{17}$$

We have checked that very similar results are obtained for other choices of $\tan\beta$, $A_0$, and $\text{sign}(\mu_{\text{SUSY}})$. Thus, our conclusions are at least valid for all MSUGRA SPS scenarios (cf. Appendix C).

In Fig. 4(a) and (b) the absolute value of the difference between the full and the approximate two-loop prediction for the Higgs boson mass, $M_h^{(2)} - M_h^{(2),\text{3lcut}}$, is shown in the $m_0$-$m_{1/2}$ plane where $M_h^{(2),\text{3lcut}}$ includes the same number of expansion terms which are available at three loops. In Fig. 4(a) we only include the results from hierarchy (h3) whereas in (b) also (h5), (h6), (h6b) and (h9) enter. For each hierarchy we compute the difference to the exact result and plot in Fig. 4(b) the minimum. We define the relative uncertainty through

$$\delta^{(2)} \quad = \quad \frac{M_h^{(2)} - M_h^{(2),\text{3lcut}}}{M_h^{(2)} - M_h^{(1)}}\,, \tag{18}$$

| | $M_h^{(2)}$ (GeV) | $M_h^{(2),\mathrm{appr}}$ (GeV) | optimal hierarchy |
|---|---|---|---|
| SPS1a | 111.81 | 111.84 | h6b |
| SPS1a′ | 113.26 | 113.27 | h6b |
| SPS1b | 115.53 | 115.64 | h3 |
| SPS2 | 115.65 | 115.77 | h5 |
| SPS3 | 114.63 | 114.77 | h3 |
| SPS4 | 113.73 | 113.77 | h6 |
| SPS5 | 111.66 | 111.83 | h3 |
| SPS7 | 112.20 | 112.21 | h3 |
| SPS8 | 114.19 | 114.20 | h3 |

Table 2: Comparison of full and approximate two-loop prediction for $M_h$ for the different benchmark points.

which is shown in Fig. 4(c) and (d). In Eq. (18) $M_h^{(i)}$ corresponds to the exact $i$-loop prediction. For reference we show in Fig. 4 the MSUGRA SPS benchmark points and slopes as (white) dots and lines, having in mind that for some of them the values of $\tan\beta$ and $A_0$ are different from the ones chosen in Eq. (16). The assignment of the individual scenarios to the corresponding dot is easily done with the help of the table in Appendix C.

Already for (h3) alone one observes a good coverage in the whole $m_0$-$m_{1/2}$ plane with deviations smaller than 150 MeV. This gets further improved after including the other hierarchies. For lower values of $m_{1/2}$ one has relative deviations also above 10%, however, the absolute difference between the full result and the approximation is below 100 MeV.

In Tab. 2 we directly compare the two-loop predictions for $M_h$ for the benchmark points listed in the table in Appendix C and SPS7 and SPS8 (gauge-mediated supersymmetry breaking) [19]. As before, the full results are based on `FeynHiggs` and Ref. [26], and for $M_h^{(2),\mathrm{appr}}$ we use the approximation incorporated in `H3m`. An impressive agreement is found, often even below 100 MeV.

The results discussed in this Subsection are very promising in view of the three-loop approximation. At two-loop order the expansion terms specified in Tab. 1 provide an excellent approximation to the full result. Thus, it can be assumed that the corresponding terms at three loops approximate the unknown result with high precision.

# 3 Technical details to the three-loop calculation

The three-loop calculation of the individual Green's functions contributing to $M_h$ is organized as follows: All Feynman diagrams are generated with `QGRAF` [31]. In order to properly take into account the Majorana character of the gluino, the output is subse-

quently manipulated by a PERL script [32] which applies the rules given in Ref. [33]. The various diagram topologies are identified and transformed to FORM [34] with the help of q2e and exp [35, 36]. The program exp is also used in order to apply the asymptotic expansion (see, e.g., Ref. [37]) in the various mass hierarchies. The actual evaluation of the integrals is performed with the package MATAD [38], resulting in an expansion in $d-4$ for each diagram, where $d$ is the space-time dimension.

The total number of three-loop diagrams amounts to 6706 and 7670 for the $\phi_1$ and $\phi_2$ self energies, respectively, and 845 and 982 for the corresponding tadpole contributions. The computation of the off-diagonal matrix element $\Sigma_{\phi_{12}}$ involves 6136 diagrams, and the propagator of the pseudoscalar Higgs another 7670. The application of the asymptotic expansion significantly enlarges these numbers leading to about 37 000 (for (h3)) or even 94 000 (for (h6)) subdiagrams. Note that there are diagrams where, depending on the hierarchy, up to 15 subdiagrams have to be considered. A typical example is shown in Fig. 1(a).

A subtlety arises from diagrams as the one shown in Fig. 1(b). If both the external momentum and the $\varepsilon$-scalar mass are set to zero from the beginning, an infra-red divergence occurs and cancels the ultra-violet divergence of the integral. In effect, the diagram will be of order $(d-4)$ due to the $\varepsilon$-scalar algebra. In order to avoid this, we keep the external momentum $q$ non-zero, though much smaller than all other scales. The ultra-violet pole multiplied by the algebraic factor of $(d-4)$ then produces a finite contribution, while the infra-red divergence leads to $(d-4)\ln(q^2)$ and vanishes as $d \to 4$.

Instead of the requirement $q \neq 0$ one could also introduce a nonzero mass for the $\varepsilon$-scalars in order to regulate the infra-red divergences. In the final result we again observe that the regulator is multiplied by an additional factor $(d-4)$ leading to a finite result for $M_\varepsilon \to 0$. We have checked that the latter prescription leads to identical results as the one with $q \neq 0$.

We refrain from presenting all available analytical results for the expansion in the various regions. They are implemented in the program H3m and thus easily accessible if necessary. However, for the convenience of the reader we provide in this Section the result for (h4), see Eq. (13), which could be useful for other applications. We will present the results expressed in terms of the $\overline{\rm DR}$ parameters $\alpha_s$, $m_t$, $m_{\tilde{t}_1}$, $m_{\tilde{t}_2}$, $m_{\tilde{g}}$ and $\theta_t$. The corresponding counterterms can be found in Appendix A.

Before providing explicit expressions a comment concerning the $\overline{\rm DR}$ renormalization constants for the top squarks is in order. Due to diagrams involving heavy squarks $\tilde{q}$, for example Fig. 5(a), the squared Higgs boson mass receives contributions which are proportional to $m^2_{\tilde{q}}$ and thus can lead to unnatural large corrections. For this reason we adopt the on-shell scheme for these contributions to $\delta Z_{m_{\tilde{t}_1}}$ and $\delta Z_{m_{\tilde{t}_2}}$ (cf. Eq. (37) and Fig. 5(b) for a sample diagram). This avoids the potentially large terms $\sim m^2_{\tilde{q}}$ from the three-loop diagrams. We follow this procedure also in the case where the top squarks and the "heavy squarks" are degenerate in mass. The renormalization of the mixing angle is free of such enhanced contributions and we can stick to the pure $\overline{\rm DR}$ scheme in that case. We hasten

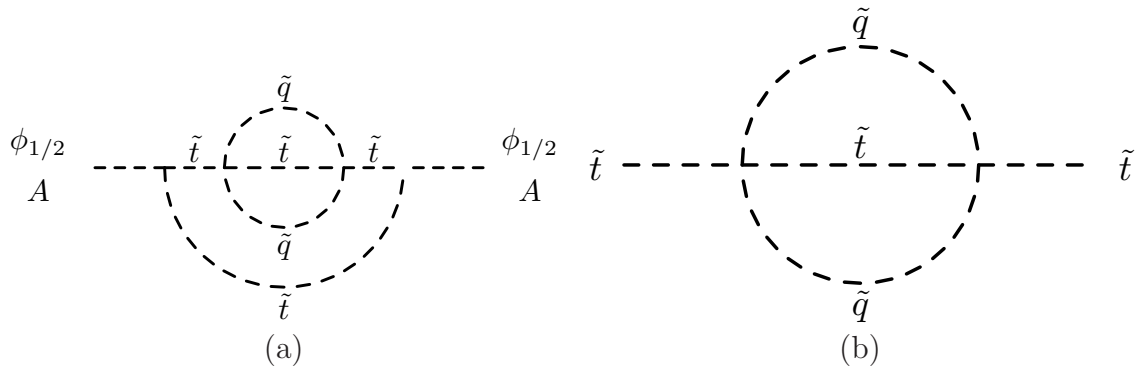


Figure 5: (a) Feynman diagram involving a heavy virtual squark contributing to the Higgs boson self energy. (b) Counterterm diagram related to the diagram in (a). The same notation as in Fig. 1 has been adopted.

to add that this discussion only concerns the internal structure of `H3m` and has no direct consequences for the user. The input parameters of `H3m` are the $\overline{\rm DR}$ ones as they appear, e.g., in the output of `SOFTSUSY`.

As already noticed in Refs. [15, 26], a similar behaviour is observed when the gluino is much heavier than the top squarks. In this case, the two- and three-loop corrections to the Higgs masses computed in the $\overline{\rm DR}$ scheme contain terms proportional to $m_{\tilde{g}}$ and $m_{\tilde{g}}^2$. These contributions are canceled in the on-shell scheme by the finite parts of the relevant counterterms. Thus, in order to avoid unnatural large radiative corrections to the Higgs masses, we adopt for scenarios with heavy gluino masses a modified renormalization scheme for the top squark masses. We call this scheme "modified $\overline{\rm DR}$" ($\overline{\rm MDR}$) and it is characterized by the non minimal renormalization of the top squark masses. The additional finite shifts of top squark masses are chosen such that they cancel the power-like behaviour of the gluino contributions. Again, the renormalization of the mixing angle will not be modified as compared to the genuine $\overline{\rm DR}$ scheme.

The relevant finite shifts for the scenarios considered in this paper are explicitly given in Appendix B. As can be noticed from Eq. (13) the scenarios (h4), (h5) and (h6) display heavy squark mass contributions whereas heavy gluino terms are specific only for the scenarios (h6) and (h6b).

In the practical calculation we use the $\overline{\rm DR}$ top squark mass parameters as provided by the spectrum generators and transform them with the help of the formulae of Appendix B to the corresponding parameters in the $\overline{\rm MDR}$ scheme which constitute the input for our analytic expressions.

In the following we present results for the renormalized two-point functions $\hat{\Sigma}_{\phi_1}$, $\hat{\Sigma}_{\phi_2}$ and

$\hat{\Sigma}_{\phi_1\phi_2}$ for the hierarchy (h4) which for equal top squark and gluino masses take the form[7]

$$
\begin{aligned}
\hat{\Sigma}_{\phi_2} = \frac{G_F m_t^4 \sqrt{2}}{\pi^2 \sin^2\beta}\Bigg[&\frac{3}{2} l_{tS} + \frac{\alpha_s}{4\pi}\Bigg(4 + \Big(4 + 16 l_{\mu t}\Big) l_{tS} + 4 l_{tS}^2 + \frac{A_t}{m_{\rm SUSY}}\Big(4 + 8 l_{\mu t} + 4 l_{tS}\Big)\Bigg) \\
&+ \Big(\frac{\alpha_s}{4\pi}\Big)^2 \Bigg\{ \frac{2764}{9} - \frac{116}{27} l_{\mu t} - \frac{136}{3} l_{\mu t}^2 + \Big( - \frac{644}{9} + \frac{164}{3} l_{\mu t}\Big) l_{tS}^2 \\
&\quad + 24 l_{tS}^3 + \frac{400}{3} l_{t\tilde{q}} - \frac{200}{3} l_{t\tilde{q}}^2 - \frac{20}{3} l_{t\tilde{q}}^3 - 120\zeta(2) - 80 l_{t\tilde{q}}\zeta(2) + \frac{8}{3}\zeta(3) \\
&\quad - \Big(\frac{2216}{27} + \frac{644}{9} l_{\mu t} - \frac{328}{3} l_{\mu t}^2 - 40 l_{t\tilde{q}} - 20 l_{t\tilde{q}}^2 - 40\zeta(2) + 16\zeta(3)\Big) l_{tS} \\
&\quad + \frac{m_{\tilde{q}}^2}{m_{\rm SUSY}^2}\Big( - 40 + 80 l_{\mu t} + 80 l_{t\tilde{q}} + 80\zeta(2)\Big) \\
&\quad + \frac{m_{\rm SUSY}^2}{m_{\tilde{q}}^2}\Bigg(\frac{42356}{225} + 8 l_{tS}^2 - \frac{2128}{45} l_{t\tilde{q}} - \frac{176}{3} l_{t\tilde{q}}^2 \\
&\qquad\qquad + \Big(\frac{3928}{45} + \frac{152}{3} l_{t\tilde{q}}\Big) l_{tS} - \frac{400}{3}\zeta(2)\Bigg) \\
&\quad + \frac{A_t m_{\rm SUSY}}{m_{\tilde{q}}^2}\Big( - 80 + l_{tS}\Big( - \frac{320}{9} - \frac{80}{3} l_{t\tilde{q}}\Big) + \frac{320}{9} l_{t\tilde{q}} + \frac{80}{3} l_{t\tilde{q}}^2 + \frac{160}{3}\zeta(2)\Big) \\
&\quad + \frac{A_t}{m_{\rm SUSY}}\Bigg(\frac{832}{27} + \frac{728}{27} l_{\mu t} + \frac{200}{3} l_{\mu t}^2 + \frac{608}{9} l_{tS}^2 \\
&\qquad\qquad + l_{tS}\Big(\frac{1256}{27} + \frac{800}{9} l_{\mu t} - \frac{160}{3} l_{t\tilde{q}}\Big) \\
&\qquad\qquad - \frac{400}{9} l_{t\tilde{q}} + 40 l_{t\tilde{q}}^2 + 80\zeta(2) - \frac{212}{3}\zeta(3)\Bigg) \\
&\quad + \frac{A_t^2}{m_{\rm SUSY}^2}\Bigg( - \frac{349}{9} + \frac{32}{9} l_{\mu t} + \frac{32}{9} l_{\mu t}^2 + \Big(\frac{56}{9} + \frac{64}{9} l_{\mu t}\Big) l_{tS} \\
&\qquad\qquad + \frac{32}{9} l_{tS}^2 + \frac{94}{3}\zeta(3)\Bigg)\Bigg\} + \mathcal{O}\left(\frac{m_{\rm SUSY}^4}{m_{\tilde{q}}^4}\right)\Bigg], \\
\hat{\Sigma}_{\phi_1} = \frac{G_F m_t^4 \sqrt{2}}{\pi^2 \cos^2\beta}&\Big(\frac{\alpha_s}{4\pi}\Big)^2 \frac{A_t^2}{m_{\rm SUSY}^2}\Bigg[ - \frac{349}{9} + \frac{32}{9} l_{\mu t} + \frac{32}{9} l_{\mu t}^2 \\
&\qquad + \Big(\frac{56}{9} + \frac{64}{9} l_{\mu t}\Big) l_{tS} + \frac{32}{9} l_{tS}^2 + \frac{94}{3}\zeta(3) + \mathcal{O}\left(\frac{m_{\rm SUSY}^4}{m_{\tilde{q}}^4}\right)\Bigg],
\end{aligned}
$$

[7] We only include terms up to order $1/m_{\tilde{q}}^2$.

$$
\begin{aligned}
\hat{\Sigma}_{\phi_{12}} = \frac{G_F m_t^4 \sqrt{2}}{\pi^2 \cos\beta \sin\beta} \Bigg[ & \frac{\alpha_s}{4\pi} \frac{A_t}{m_{\rm SUSY}} \Big( -2 - 4 l_{\mu t} - 2 l_{tS} \Big) \\
& + \Big( \frac{\alpha_s}{4\pi} \Big)^2 \Bigg\{ \frac{A_t^2}{m_{\rm SUSY}^2} \left( \frac{349}{9} - \frac{32}{9} l_{\mu t} - \frac{32}{9} l_{\mu t}^2 + \Big( -\frac{56}{9} - \frac{64}{9} l_{\mu t} \Big) l_{tS} - \frac{32}{9} l_{tS}^2 - \frac{94}{3} \zeta(3) \right) \\
& \quad + \frac{A_t m_{\rm SUSY}}{m_{\tilde{q}}^2} \left( 40 - \frac{160}{9} l_{t\tilde{q}} - \frac{40}{3} l_{t\tilde{q}}^2 + l_{tS} \Big( \frac{160}{9} + \frac{40}{3} l_{t\tilde{q}} \Big) - \frac{80}{3} \zeta(2) \right) \\
& \quad + \frac{A_t}{m_{\rm SUSY}} \Big( -\frac{416}{27} - \frac{364}{27} l_{\mu t} - \frac{100}{3} l_{\mu t}^2 - \frac{304}{9} l_{tS}^2 + \frac{200}{9} l_{t\tilde{q}} - 20 l_{t\tilde{q}}^2 \\
& \quad + l_{tS} \Big( -\frac{628}{27} - \frac{400}{9} l_{\mu t} + \frac{80}{3} l_{t\tilde{q}} \Big) - 40\zeta(2) + \frac{106}{3} \zeta(3) \Big) \Bigg\} + \mathcal{O}\left( \frac{m_{\rm SUSY}^4}{m_{\tilde{q}}^4} \right) \Bigg] ,
\end{aligned}
$$

with $m_t = m_t(\mu_r)$, $m_{\rm SUSY} = m_{\rm SUSY}(\mu_r) = m_{\tilde{t}_1}(\mu_r) = m_{\tilde{t}_2}(\mu_r) = m_{\tilde{g}}(\mu_r)$, $l_{\mu t} = \ln(\mu_r^2/m_t^2)$, $l_{tS} = \ln(m_t^2/m_{\rm SUSY}^2)$ and $l_{t\tilde{q}} = \ln(m_t^2/m_{\tilde{q}}^2)$ where $\mu_r$ is the renormalization scale. The on-shell result corresponding to $\hat{\Sigma}_{\phi_2}$ has been presented in Ref. [12] for $A_t = 0$.

We refrain from providing more analytic results since all of them come along with the program `H3m` which is discussed in the next section.

# 4 Description of `H3m`

In this Section we describe the implementation of our three-loop results in a user-friendly computer program which allows the evaluation of the light CP even Higgs boson mass $M_h$ to three-loop accuracy. The program is implemented in the form of a `Mathematica` package.

To set the input parameters for the calculation, i.e. the SUSY spectrum and SM parameters, the SUSY Les Houches Accord (SLHA) [39] is used. For ease of use, we provide functions that call a spectrum generator from `Mathematica` to produce an SLHA spectrum file. To produce the plots in this publication, we have chosen `SOFTSUSY` [27], but it is possible to use any spectrum generator that provides the $\overline{\rm DR}$ parameters in addition to the on-shell mass spectrum like `SuSpect` [40] or `SPheno` [41]. The advantage of `SOFTSUSY` is that the renormalization scale of the $\overline{\rm DR}$ parameters can be chosen independently of the electroweak symmetry breaking.

The corrections $\Delta^{m_t^4} M_h$ to $M_h$, being proportional to the fourth power of the mass of the top quark $m_t$, are very sensitive to both the definition and the uncertainty of $m_t$. Thus, it is important to use the most precise value of $m_t$ available. For this reason we take into account the full two-loop SQCD corrections between the on-shell and $\overline{\rm DR}$ top quark mass given in Ref. [42].[8] In this paper, the relation of the on-shell top mass $M_t$ and $\overline{\rm DR}$ top mass $m_t$ was derived as a function of the $\overline{\rm DR}$ masses. Solving this equation iteratively,

[8] We thank Steven Martin for providing us with the relevant formulae from Ref. [42] in electronic form, and for allowing us to include his code in our program.

we get $m_t$ as a function of $M_t$. The integrals appearing in [42] are evaluated using the `C` library `TSIL` [43]. This relation is available for general renormalization scale $\mu_r$ which enables us to obtain $m_t(\mu_r)$ in the $\overline{\rm DR}$ scheme using the on-shell mass $M_t$ as measured at the Tevatron [44] as input.

Another critical parameter for the evaluation of $M_h$ is the strong coupling $\alpha_s$. We use $\alpha_s(M_Z)$ as input and follow Ref. [45–47] in order to evaluate $\alpha_s$ in the $\overline{\rm DR}$ scheme with all SUSY particles contributing to the running. First, $\alpha_s^{(5),\overline{\rm MS}}(M_Z) = 0.1184$ [48] is run up to the decoupling scale, which we set to the average value of the SUSY particles, using the four-loop $\beta$ function [49, 50]. There, we perform the transition to the $\overline{\rm DR}$ scheme and the full theory. The two-loop matching coefficients from [47] are used in this step. To obtain $\alpha_s^{(\rm full),\overline{\rm DR}}(\mu_r)$ for arbitrary values of the renormalization scale $\mu_r$, we use the three-loop SQCD $\beta$ function given in [51, 32].

The remaining input parameters comprise the ones for the SUSY breaking scenario, which we summarise in the table of Appendix C and the SM parameters $M_Z$, $G_F$ and $\alpha$ which also serve as input for the spectrum. The default values set in `H3m` read

$$\begin{aligned} M_Z &= 91.1876 \text{ GeV}, \\ M_t &= 173.1 \text{ GeV}, \\ G_F &= 1.16637 \cdot 10^{-5} \text{ GeV}^{-2}, \\ 1/\alpha(M_Z) &= 127.934, \\ \alpha_s(M_Z) &= \alpha_s^{(5),\overline{\rm MS}}(M_Z) = 0.1184. \end{aligned} \tag{19}$$

Of course, it is possible to modify these default values. Note that the top squark masses and mixing angle are obtained from the soft breaking parameters according to Eqs. (9) and (11).

In order to include all the known corrections to $M_h$ at the one- and two-loop level, the spectrum file is passed to `FeynHiggs` [9, 13–15]. `FeynHiggs` uses on-shell parameters that are given in the spectrum file and provides the neutral Higgs mass matrix up to the two-loop level. Since we prefer to use the $\overline{\rm DR}$ scheme, we need to perform a conversion before adding our three-loop results. This we do by subtracting the on-shell expression for $\Delta^{m_t^4} M_h$ (up to two loops, without any expansions in the masses[9]) and adding it back in the $\overline{\rm DR}$ scheme. Thus, we use the $\overline{\rm DR}$ scheme to evaluate $\Delta^{m_t^4} M_h$, which are dominant and sensitive to the top quark mass, and the on-shell scheme for $\Delta^{\rm rem} M_h$.

The next step is to choose a suitable mass hierarchy for the expansion of the three-loop corrections. This is done by comparing, at the two-loop level, the full result from Ref. [26] with the expansions in all the mass hierarchies and choosing the one minimizing the error. Finally, the three-loop corrections are added, the neutral Higgs mass matrix is diagonalized, and the mass of the light Higgs is returned to the user.

The interface of the program is outlined in Fig. 6. The parameters are set up by a call of

[9] We thank Pietro Slavich for sending us the compact formulae from Ref. [26] in electronic form.

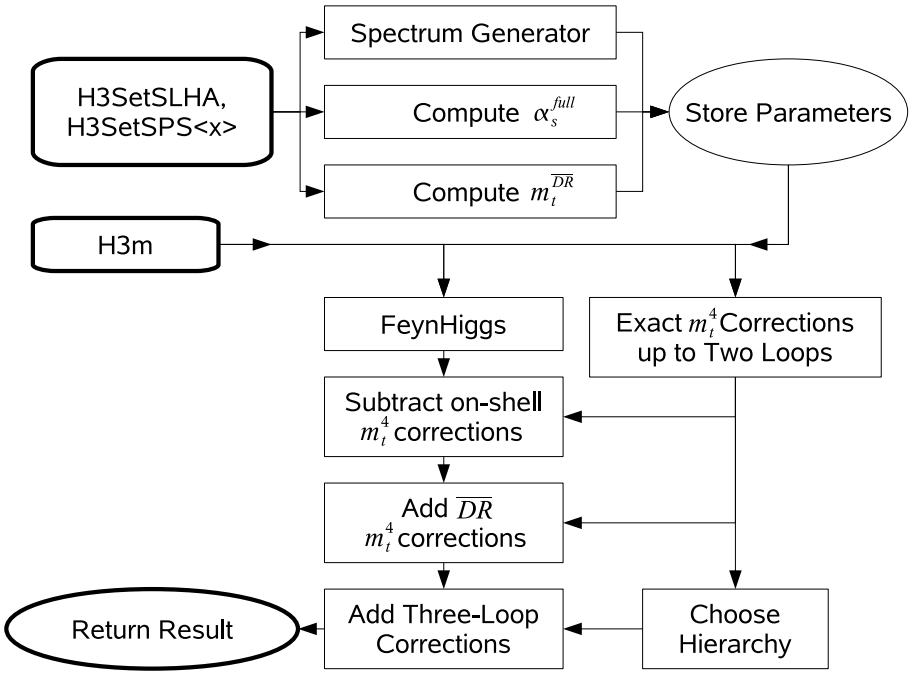


Figure 6: Flowchart of `H3m`. First, the user calls `H3SetSLHA` or one of its descendants to set the parameters. A subsequent call to `H3m`computes $M_h$.

the function `H3SetSLHA`, which passes its arguments to the spectrum generator and parses its output to get the relevant input parameters for the calculation. The top mass and strong coupling are calculated as described above. Alternatively, the function `H3GetSLHA` uses an existing spectrum file instead of running a generator. For the user interested in the Snowmass Points and Slopes, we provide convenient wrapper functions `H3SetSPS<x>` which call `H3SetSLHA` with parameters according to a specific benchmark scenario.

The main calculation is organized by the function `H3m`, which calls `FeynHiggs`, does the conversion to the $\overline{\rm DR}$ scheme described above, chooses an appropriate mass hierarchy, adds the three-loop corrections, and returns $M_h$.

In Fig. 7, a typical `Mathematica` session with `H3m` is shown. A more detailed description of `H3m` comes along with the program which can be found at the web page [21].

# 5 The Higgs boson mass to three-loop accuracy

In this Section we use, if not stated otherwise, the input parameters as listed in Eq. (19) and furthermore adopt for the renormalization scale $\mu_r = M_t$ as our default value.

In Fig. 8 we show the renormalization scheme dependence of $M_h$ as a function of $m_{1/2}$ for the SPS2 scenario. This is convenient since we have the same abscissa both for the on-shell

```
Mathematica 7.0 for Linux x86 (64-bit)
Copyright 1988-2008 Wolfram Research, Inc.

In[1]:= Needs["H3`"];

RunDec: a Mathematica package for running and decoupling of the
        strong coupling and quark masses
by K.G. Chetyrkin, J.H. Kuhn and M. Steinhauser (January 2000)

In[2]:= H3SetSPS1a[ 300.];

H3GetSLHA::TSIL: Using TSIL by S.P. Martin.
 ------------------------------------------------------
 FeynHiggs 2.6.5
 built on Dec 20, 2008
 T. Hahn, S. Heinemeyer, W. Hollik, H. Rzehak, G. Weiglein
 http://www.feynhiggs.de
 ------------------------------------------------------
 FHHiggsCorr contains code by:
 P. Slavich et al. (2-loop rMSSM Higgs self-energies)
Loading Results for hierarchy h3
Loading Results for hierarchy h3
Loading Results for hierarchy h6b2qg2
Loading Results for hierarchy h6b2qg2

In[3]:= H3m[]

Loading Results for hierarchy h6b2qg2

Out[3]= {mh -> 114.176}
```

Figure 7: A typical `Mathematica` session with `H3m`.

and $\overline{\rm DR}$ result. Note, however, that the three-loop on-shell result is only available for a degenerate mass spectrum of the SUSY particles and vanishing parameter $A_t$ [12]. Thus, we restrict ourselves to this limit also for the $\overline{\rm DR}$ result. For this reason the following discussion should be considered in a less quantitative but more qualitative sense and should not be used, e.g., for estimating a theoretical uncertainty.

In the left panel of Fig. 8 the upper dotted, dashed and solid curve correspond to the one-, two- and three-loop prediction of $M_h$ in the on-shell scheme whereas the corresponding lower three curves are obtained in the $\overline{\rm DR}$ scheme. In the on-shell scheme one observes large positive one-loop corrections which get reduced by 10 to 20 GeV after including the

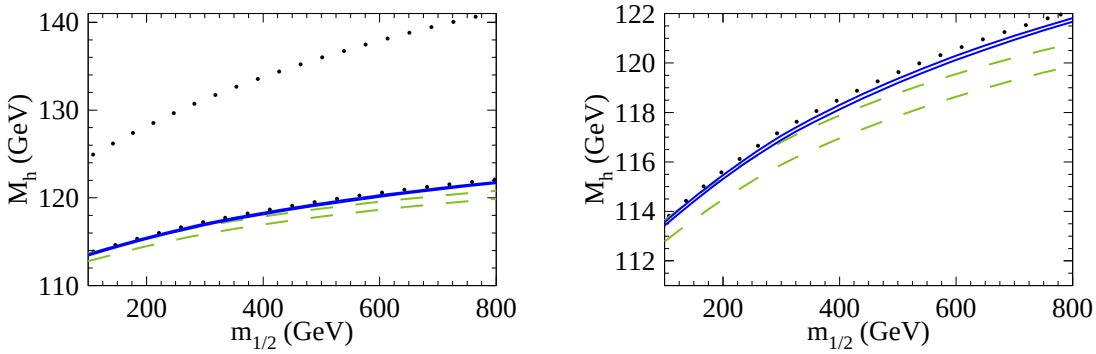


Figure 8: Renormalization scheme dependence of $M_h$ as a function of $m_{1/2}$ adopting SPS2. Dotted, dashed and solid curves correspond to one-, two- and three-loop results. The $\overline{\rm DR}$ (on-shell) results correspond to the lower (upper) three curves. In the right panel the interesting part of the left one is magnified.

two-loop terms. The three-loop corrections amount to several hundred MeV. They are positive or negative — depending on the value of $m_{1/2}$.

The situation is completely different for $\overline{\rm DR}$ mass parameters: the one-loop corrections are significantly smaller and lead to values of $M_h$ which are already of the order of the two- and three-loop on-shell prediction. The two-loop term leads to a small shift of the order of $-1$ GeV and the three-loop term to a positive shift of about the same order of magnitude. The final prediction for $M_h$ is very close to the one obtained after incorporating three-loop on-shell results.[10]

Comparing the $\overline{\rm DR}$ and on-shell results in Fig. 8 one observes a nice reduction of the scheme dependence when incorporating higher order corrections.[11] Whereas there is a huge gap between the two one-loop curves (dotted) the difference in the two-loop prediction of $M_h$ is below 2 GeV which gets further reduced by about a factor ten after incorporating the three-loop corrections to roughly 200 MeV.

Fig. 9 extends Fig. 4 to three loops. In (a) and (b) we again discuss the hierarchy (h3) and the combination of the hierarchies (h3), (h5), (h6), (h6b) and (h9), respectively, and show the difference between our best prediction and the one where the expansion parameters are cut by one unit.[12] In the whole parameter plane we observe small absolute corrections reaching at most about 100 MeV. This leads to the conclusion that as a conservative estimate of the uncertainty of our approximation procedure one can assign about 100 MeV.

[10]The relatively large three-loop corrections (as compared to the two-loop ones) do not pose any problem since we use simplified formulae as mentioned before. Furthermore, there are regions in the parameter space where the two-loop corrections are accidentally small in the $\overline{\rm DR}$ scheme leading to large relative three-loop terms. Nevertheless the overall size of the two- and three-loop corrections is small.

[11]Up to two-loop order the scheme dependence has already been discussed in Fig. 2.

[12]We only cut in parameters originating from asymptotic expansion: when counting powers of mass ratios, we leave $\sin 2\theta_t$ untouched and do not replace it by Eq. (11).

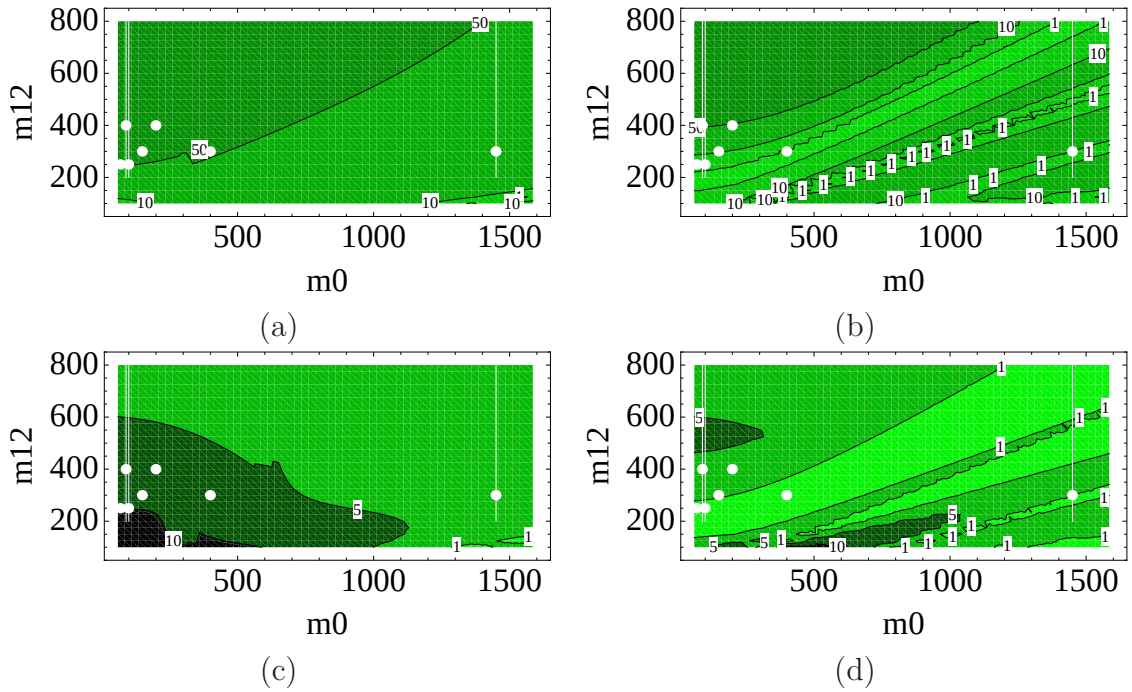


Figure 9: Comparison of the three-loop predictions for $M_h$ using the maximal available expansion terms and reduced input as described in the text. In (a) and (b) the absolute deviations are shown for the hierarchy (h3) and the combination of (h3), (h5), (h6), (h6b) and (h9), respectively. The contour lines indicate the deviations in MeV. In (c) and (d) the results of (a) and (b) are normalized to the genuine three-loop contributions where the contour lines indicate the deviations in per cent. The benchmark points and slopes are shown as (white) dots and lines.

In Fig. 9(c) and (d) we show relative deviations defined through

$$\delta^{(3)} \quad = \quad \frac{M_h^{(3)} - M_h^{(3),\mathrm{cut}}}{M_h^{(3)} - M_h^{(2)}}\,, \tag{20}$$

where $M_h^{(3)}$ is our best three-loop prediction, $M_h^{(3),\mathrm{cut}}$ is the prediction where at three-loop order the expansion depth of each parameter (cf. Tab. 1) is reduced by one unit, and $M_h^{(2)}$ corresponds to the (full) two-loop term. Similar to the two-loop case, larger corrections are only observed for small values of $m_0$ and $m_{1/2}$ which is a consequence of a small denominator in Eq. (20). The three-loop correction terms, however, are stable as can be seen from the panels (a) and (b). Thus, as in the two-loop case, we are able to cover the whole $m_0$-$m_{1/2}$ plane and are in particular able to produce precise values for $M_h$ for all SPS scenarios.

The slopes for three SPS scenarios are shown in Fig. 10(a), (b) and (c) where the dotted, dashed and solid lines correspond to the one-, two- and three-loop predictions, respectively. For all three cases one observes negative corrections between 1 and 4 GeV at two loops

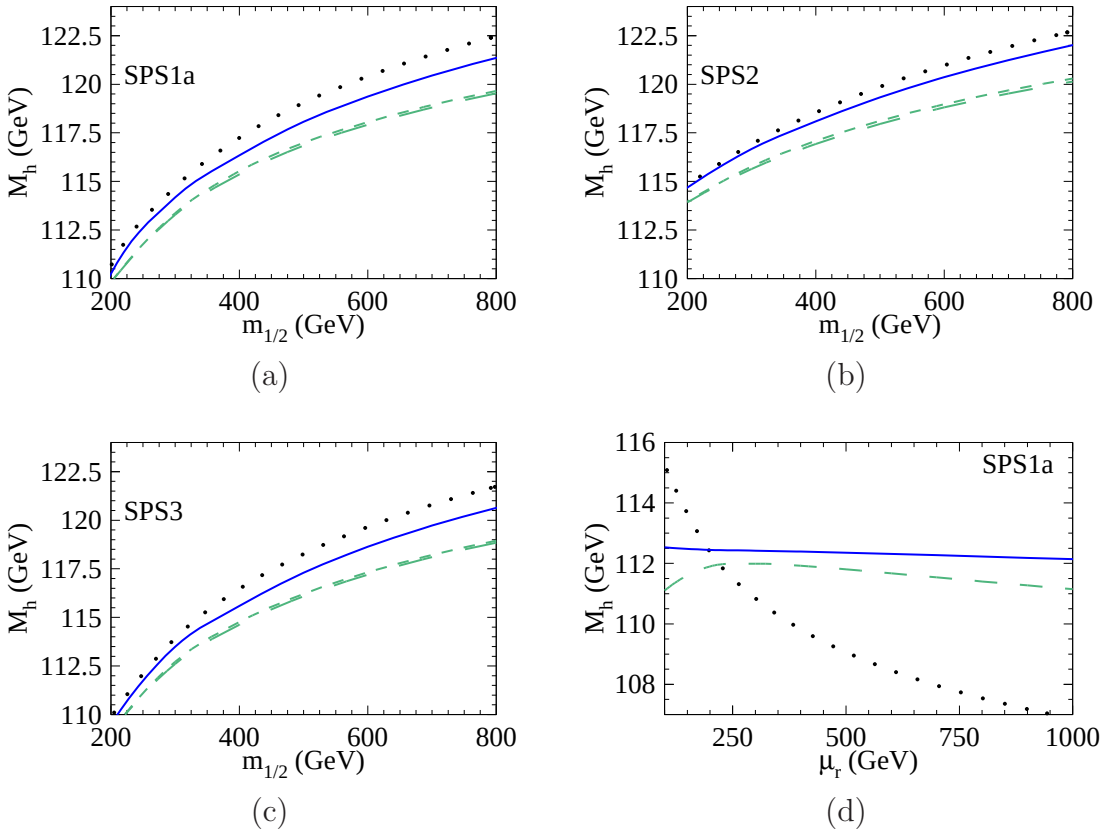


Figure 10: $M_h$ for the different slopes of the benchmark scenarios SPS1a (a), SPS2 (b) and SPS3 (c). Dotted, dashed and solid lines correspond to the one-, two- and three-loop predictions. The dashed line with longer dashes (at two loops) correspond to the full results, the one with the shorter dashes to the approximation implemented in `H3m`. In (d) the dependence of $M_h$ on the renormalization scale is shown where the dotted, dashed and solid line corresponds to the one-, two- and three-loop prediction.

and positive contributions from the three-loop term which amount up to about 2 GeV.

In Fig. 10(d) we show the dependence of the prediction for $M_h$ on the renormalization scale $\mu_r$. As an example we adopt the SPS1a scenario with $m_{1/2} = 250$ GeV and exploit that `SOFTSUSY` allows the evaluation of all $\overline{\rm DR}$ parameters at the scale $\mu_r$. One observes a strong dependence at one-loop order which gets significantly reduced at two loops. The three-loop curve is even more flat resulting in a stable prediction for $M_h$. Around $\mu_r = 250$ GeV the two-loop correction shows a local maximum and is furthermore very small whereas the three-loop term still amounts to about 500 MeV. Around $\mu_r = M_t$, which is often used as a default choice, one has negative two-loop corrections of about $-2$ GeV and a slightly larger three-loop contribution than for $\mu_r = 250$ GeV. The corresponding plots for SPS2 and SPS3 look very similar. Thus, we refrain from presenting them here; they can easily be generated with the help of `H3m`.

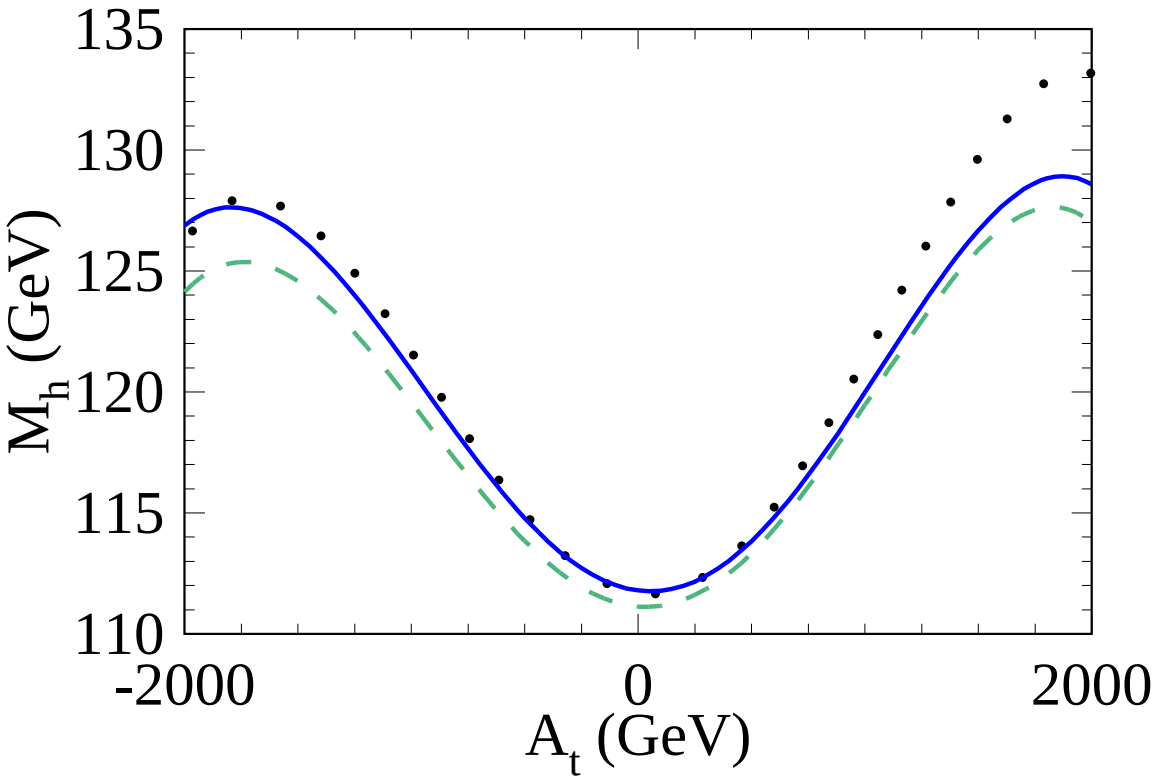


Figure 11: Dependence of $M_h$ on $A_t$. The dotted, dashed and solid line corresponds to the one-, two- and three-loop prediction.

It is interesting to investigate the dependence of $M_h$ on the soft breaking parameter $A_t$. In Fig. 11 we show the result for $M_h$ where the following values for the parameters have been chosen

$$\begin{aligned} m_{\tilde{t}_1} &= 500 \text{ GeV}, \\ m_{\tilde{t}_2} &= 1000 \text{ GeV}, \\ m_{\tilde{g}} &= 500 \text{ GeV}, \\ m_{\tilde{q}} &= 2000 \text{ GeV}, \\ \mu_{\text{SUSY}} &= 800 \text{ GeV}, \\ \tan\beta &= 10, \\ M_A &= 1500 \text{ GeV}. \end{aligned} \tag{21}$$

Furthermore, we employ only the $m_t^4$ corrections since it is not possible to transmit the parameters of Eq. (21) directly to `FeynHiggs` and evaluate the corresponding Higgs boson mass.

It is interesting to note that the three-loop corrections are quite sizeable, amounting

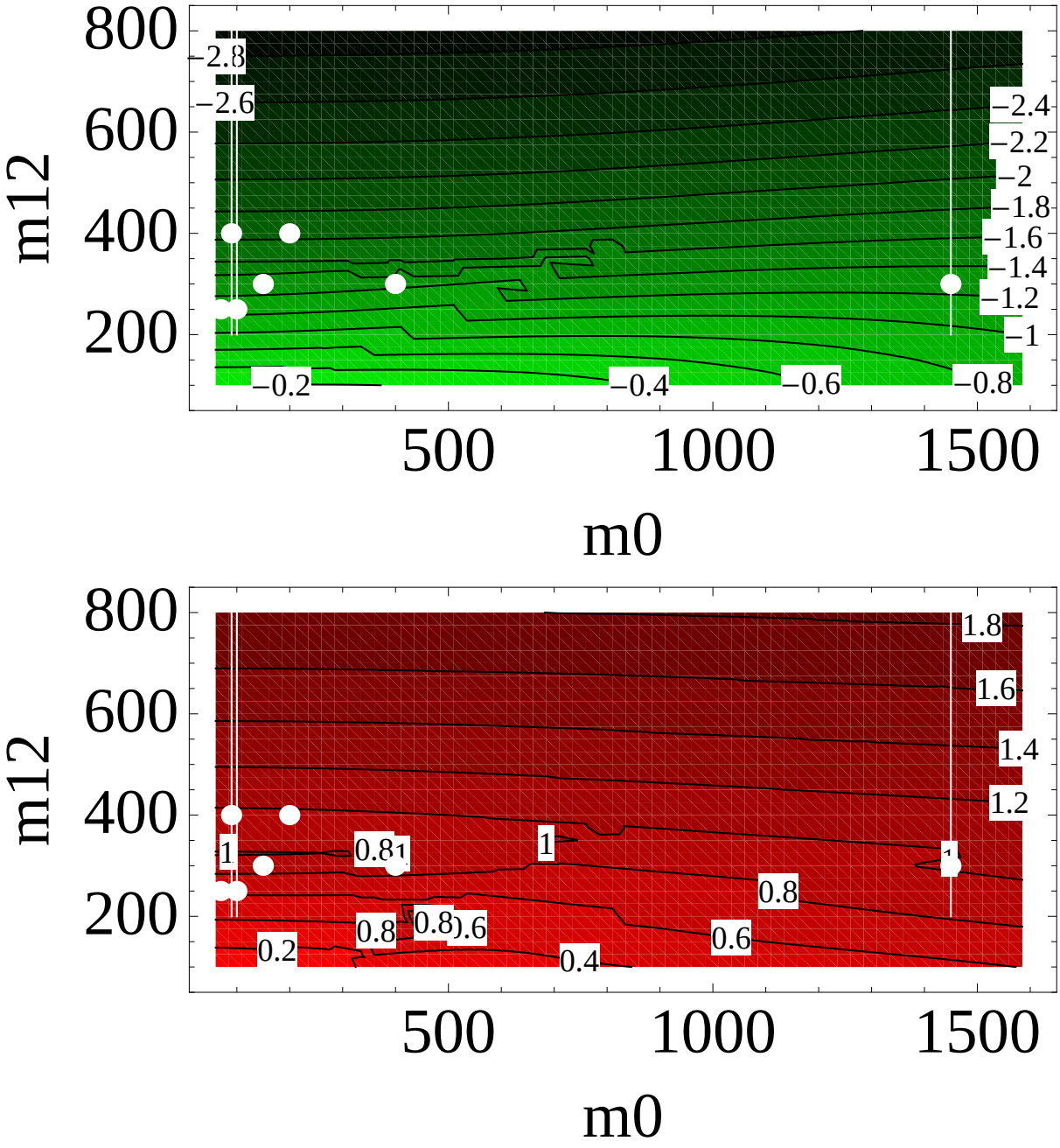


Figure 12: Genuine two- (upper panel) and three-loop (lower panel) corrections to $M_h$ in the $m_0$-$m_{1/2}$ plane.

up to about 3 GeV. In contrast to the two-loop terms they are positive and lead to a compensation. For $A_t = -2\,\text{TeV}$ and $A_t = 0$ the three-loop prediction is even above the one-loop value for $M_h$.

In order to get an impression on the size of the three-loop corrections we show in Fig. 12

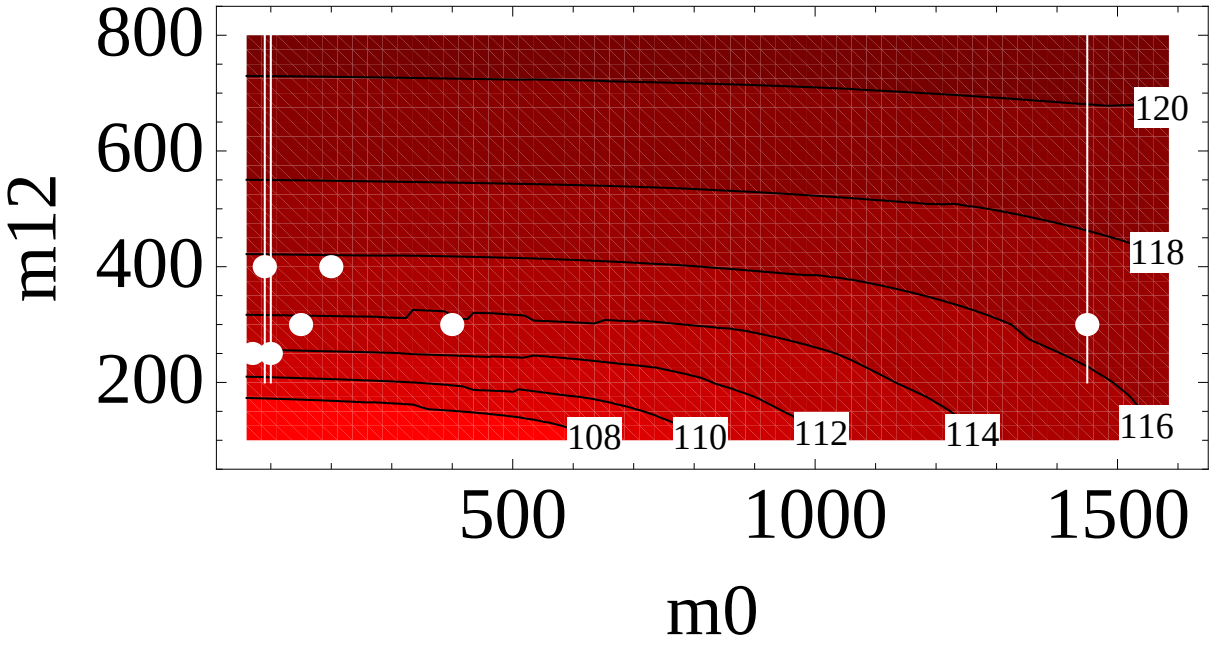


Figure 13: Prediction of $M_h$ to three-loop accuracy using `H3m`. The same conventions as in Fig. 12 have been adopted.

(lower panel) the difference between our best three-loop prediction and the full two-loop result as a function of $m_0$ and $m_{1/2}$. We observe that the corrections are always positive and vary for our parameters between a few hundred MeV and about 2 GeV. They show only a mild dependence on $m_0$, but vary strongly with $m_{1/2}$. In particular the corrections become larger for increasing values of $m_{1/2}$. For comparison, we show in Fig. 12 (upper panel) the corresponding quantity at two-loop order, i.e., the difference between the two-loop and the one-loop result. In contrast to the three-loop contributions they are negative and amount to about twice the three-loop terms in a large region of the parameter space. However, there are also regions where the three-loop corrections are larger than the two-loop ones. Note, however, that in the whole $m_0$-$m_{1/2}$ plane the one-loop corrections are more than ten times bigger. Furthermore, the occurrence of three-loop corrections, which are large compared to the two-loop ones, can also be seen from Fig. 10(d): whereas the two-loop corrections vary between $-4$ GeV and $+4$ GeV in the considered range of $\mu_r$ the three-loop term is almost constant and amounts to about 1 GeV relative to the two-loop result.

In Fig. 13 we finally show the three-loop prediction of $M_h$ including the three-loop effects discussed in this paper. Again we restrict ourselves to the parameter space defined above. Values for other input parameters are easily obtained with the help of `H3m`. One can see that for increasing $m_{1/2}$ also the Higgs boson mass gets larger and values well above 120 GeV can be reached. This is already observed at one-loop order and is due to the fact that for larger values of $m_{1/2}$ the whole supersymmetric spectrum becomes heavier.

| | $M_h^{(3)}$ (GeV) | $M_h^{(3),\rm cut}$ (GeV) | optimal hierarchy |
|---|---|---|---|
| SPS1a | 112.46 | 112.45 | h6b |
| SPS1a′ | 113.92 | 113.92 | h6b |
| SPS1b | 116.49 | 116.44 | h3 |
| SPS2 | 116.67 | 116.61 | h5 |
| SPS3 | 115.59 | 115.52 | h3 |
| SPS4 | 114.82 | 114.81 | h6 |
| SPS5 | 112.02 | 111.92 | h3 |
| SPS7 | 113.04 | 113.04 | h3 |
| SPS8 | 115.03 | 115.02 | h3 |

Table 3: Comparison of the best three-loop prediction to the one where some expansion parameters are cut (see text). The last column shows the chosen hierarchy.

| scenario | 1 loop | 2 loops | 3 loops |
|---|---|---|---|
| $m_h^{\rm max}$ | 141.11 | 133.96 | 134.38 |
| no-mixing | 121.33 | 119.72 | 121.07 |
| gluophobic | 118.52 | 117.47 | 117.29 |
| small $\alpha_{\rm eff}$ | 120.20 | 118.33 | 119.10 |

Table 4: Results for $M_h$ (in GeV) for the benchmark scenarios defined in Ref. [52] where $\tan\beta = 10$ and $M_A = 1500$ GeV has been chosen.

For definiteness we show in Tab. 3 the three-loop prediction of $M_h$ for the SPS points. We show the best prediction ($M_h^{(3)}$) and, for comparison, the result obtained by cutting parameters as for Fig. 9 ($M_h^{(3),\rm cut}$). Furthermore, we indicate the optimal hierarchy as chosen by `H3m`. In all cases the uncertainty due to our approximation can be estimated to be below 100 MeV.

As a last phenomenological application we consider the benchmark points identified in Ref. [52] in order to perform the MSSM Higgs boson search at hadron colliders. In Tab. 4 the one-, two- and three-loop predictions for $M_h$ are shown for the four scenarios "$m_h^{\rm max}$", "no-mixing", "gluophobic" and "small $\alpha_{\rm eff}$". Whereas for "no-mixing" significant three-loop effects are observed more moderate, however, still important contributions are obtained for the remaining three scenarios. In Tab. 4 $\tan\beta = 10$ and $M_A = 1500$ GeV has been chosen, however, a similar conclusion can be drawn for other values.

Let us at the end of this Section estimate the theoretical uncertainty on the prediction of $M_h$ after including the three-loop corrections. We divide the uncertainty into two parts: ($i$) the theoretical error due to missing higher order corrections and other as of yet uncalculated corrections, and ($ii$) the parametric uncertainty, mainly due to the top quark mass, $\alpha_s$ and the supersymmetric masses. At two-loop level, a thorough investigation

of the theoretical uncertainties (i) has been performed in Ref. [8] (for earlier work, see Ref. [14]). It was found that missing two-loop corrections (most importantly electro-weak and finite-momentum effects) can be assumed to be well below 1 GeV, while the as of then unknown three-loop effects could amount to 2-3 GeV, as indicated by the variation of the two-loop results with the renormalization scale.

With the $\alpha_t\alpha_s^2$ corrections of our calculation, we should therefore be able to reduce the theory uncertainty. Instead of renormalization scale variations, however, we want to adopt a more conservative attitude and assume a geometric progression of the perturbative series. As can be confirmed at two-loop level, a conservative estimate of the uncertainty is 50% of the difference to the next lower order. Thus we assign 50% of the three-loop contribution to $M_h$ as a theoretical error. For the MSUGRA scenarios this leads to an uncertainty of about $100 - 200$ MeV for $m_{1/2} = 100$ GeV and to about 1 GeV for $m_{1/2} = 1$ TeV. These estimates cover also corrections from renormalization group improvements which at two-loop order lead to shifts in $M_h$ of the order of a few GeV [**?**].

Earlier in this section, we have identified two more contributions to the uncertainties of type (i): The corrections beyond the quartic top quark mass contribution, $\Delta^{\rm rem}M_h^{(3)}$, has been estimated to about 100 MeV and the uncertainty due to our approximation procedure also amounts to at most 100 MeV. Both contributions are smaller than the one due to missing higher order corrections discussed above.

The parametric uncertainties can be easily estimated with the help of `H3m`. For definiteness we adopt in the following SPS2 and vary $M_t$ and $\alpha_s(M_Z)$ as follows

$$M_t = 173.1 \pm 1.3 \text{ GeV}, \tag{22}$$

$$\alpha_s(M_Z) = 0.1184 \pm 0.0020. \tag{23}$$

In the case of the top quark mass we observe for $m_{1/2} = 100$ GeV a variation of $M_h$ by about 350 MeV which increases to $\delta M_h = 1$ GeV for $m_{1/2} = 1$ TeV. The corresponding numbers for the uncertainty in $\alpha_s(M_Z)$ read 80 MeV and 600 MeV. A further uncertainty is connected to the (unknown) supersymmetric parameters which may also be of the order of a few hundred MeV. Assuming, e.g., an uncertainty of 10% for $m_{\tilde{t}_1}$ in the range between 200 and 800 GeV and adopting the remaining parameters from Eq. (21) leads to an uncertainty of at most 500 MeV for $M_h$. Note that the parametric uncertainty is of the same order of magnitude as the theoretical error due to missing higher order corrections as estimated in the previous paragraph.

# 6 Conclusions

In this paper we have discussed the lightest Higgs boson mass of the MSSM to three-loop accuracy. At this order an exact calculation is out of range and thus we heavily exploit the methods of asymptotic expansion in order to provide precise approximations. This procedure has been successfully tested at two-loop order against the full result. The result

is expressed in terms of $\overline{\rm DR}$ parameters for the quark and squark masses for which we have found very good convergence of the perturbative expansion. We provide a user-friendly `Mathematica` program `H3m` which allows the computation of $M_h$ in a simple way. In particular, it is possible to apply various SUSY breaking scanarios, invoke a spectrum generator, and use the output in order to compute $M_h$.

As already mentioned, with the help of the asymptotic expansion we have implemented analytical results valid for various hierarchies in the supersymmetric masses. `H3m` is set up in such a way that it is straightforward to include further hierarchies in case they are needed for future investigations.

We have performed several studies with the new three-loop corrections. In particular, we have considered their renormalization scheme and scale dependence, and their numerical effect in the various SPS scenarios. Furthermore, assuming MSUGRA, we have considered the $m_0$-$m_{1/2}$ parameter space and computed two and three-loop corrections. On the basis of these investigations we estimate the remaining theory uncertainty of $M_h$ to about 200 MeV for $m_{1/2} = 100$ GeV and to about 1 GeV for $m_{1/2} = 1$ TeV.

# Acknowledgements

We thank Steven Martin for providing us with `C++` routines for the relation between the $\overline{\rm DR}$ and on-shell top quark mass, and Pietro Slavich for providing us with the analytic result for the two-loop SQCD corrections. We are grateful to Sven Heinemeyer for carefully reading the manuscript and many valuable comments, and to Thomas Hermann for useful comments on Appendix A. This work was supported by the DFG through SFB/TR 9 "Computational Particle Physics" and contract HA 2990/3-1, and by the Helmholtz Alliance "Physics at the Terascale".

# Appendix A: $\overline{\rm DR}$ counterterms

In this appendix we provide details about the computation of the counterterms for the gluino, top quark and squark masses and the mixing angle in the top squark system.

To define our framework for the computation of the top squark masses and mixing angle counterterms, we start from the bare Lagrangian containing the kinetic energy and mass terms

$$\mathcal{L}_{\tilde{t}}^{(0)} = \frac{1}{2}\partial_\mu(\tilde{t}_L^*, \tilde{t}_R^*)^{(0)}\partial^\mu \begin{pmatrix} \tilde{t}_L \\ \tilde{t}_R \end{pmatrix}^{(0)} - \frac{1}{2}(\tilde{t}_L^*, \tilde{t}_R^*)^{(0)}(\mathcal{M}_{\tilde{t}}^2)^{(0)} \begin{pmatrix} \tilde{t}_L \\ \tilde{t}_R \end{pmatrix}^{(0)}, \tag{24}$$

where the superscript (0) labels the bare quantities, $\tilde{t}_L$ and $\tilde{t}_R$ denote the interaction eigenstates and the top squark mass matrix was defined in Eq. (8).

The top squark mass eigenstates are related to the interaction eigenstates by

$$\begin{pmatrix} \tilde{t}_1 \\ \tilde{t}_2 \end{pmatrix}^{(0)} = \mathcal{R}_{\tilde{t}}^{(0)\,\dagger} \begin{pmatrix} \tilde{t}_L \\ \tilde{t}_R \end{pmatrix}^{(0)} , \tag{25}$$

where the matrix $\mathcal{R}_{\tilde{t}}$ is defined in Eq. (10).

The wave function renormalization can be written in matrix form

$$\begin{pmatrix} \tilde{t}_1 \\ \tilde{t}_2 \end{pmatrix}^{(0)} = \mathcal{Z}_{\tilde{t}}^{1/2} \begin{pmatrix} \tilde{t}_1 \\ \tilde{t}_2 \end{pmatrix} , \quad \text{with} \quad \mathcal{Z}_{\tilde{t}}^{1/2} = \begin{pmatrix} Z_{11}^{1/2} & Z_{12}^{1/2} \\ Z_{21}^{1/2} & Z_{22}^{1/2} \end{pmatrix} , \tag{26}$$

where we have $\mathcal{Z}_{\tilde{t}}^{1/2} = \mathbf{I} + \mathcal{O}(\alpha_s)$. Thus, $Z_{11}^{1/2} = 1 + \mathcal{O}(\alpha_s)$, $Z_{22}^{1/2} = 1 + \mathcal{O}(\alpha_s)$, $Z_{12}^{1/2} = \mathcal{O}(\alpha_s)$ and $Z_{21}^{1/2} = \mathcal{O}(\alpha_s)$.
Similarly, the renormalized mass matrix can be parametrized as follows

$$\begin{pmatrix} m_{\tilde{t}_1}^2 & 0 \\ 0 & m_{\tilde{t}_2}^2 \end{pmatrix}^{(0)} = \begin{pmatrix} m_{11}^2 Z_{m_{11}} & m_{12}^2 Z_{m_{12}} \\ m_{21}^2 Z_{m_{21}} & m_{22}^2 Z_{m_{22}} \end{pmatrix} \equiv \mathcal{M} , \tag{27}$$

where the $m_{ij}$ stand for renormalized mass parameters.

In order to extract the renormalization constants it is convenient to consider the renormalized inverse top squark propagator which reads

$$iS^{-1}(p^2) = p^2 (\mathcal{Z}_{\tilde{t}}^{1/2})^\dagger \mathcal{Z}_{\tilde{t}}^{1/2} - (\mathcal{Z}_{\tilde{t}}^{1/2})^\dagger [\mathcal{M} - \Sigma(p^2)] \mathcal{Z}_{\tilde{t}}^{1/2} , \tag{28}$$

where $\Sigma(p^2)$ denotes the matrix of self energies constructed by the $\tilde{t}_1$ and $\tilde{t}_2$ fields.

To determine the renormalization constants introduced above one has to specify the renormalization conditions. In the $\overline{\rm DR}$ scheme the finite parts of the renormalization constants are set to zero and the coefficients of the $\epsilon$ poles are obtained from the requirements

$$\begin{aligned} iS_{ij}^{-1}(p^2)\Big|_{\rm pp} &= 0 , \\ m_{12}^2 Z_{m_{12}} = m_{21}^2 Z_{m_{21}} &= 0 , \end{aligned} \tag{29}$$

where "pp" stands for the "pole part". The conditions in the second line of Eq. (29) ensure that the renormalized fields $\tilde{t}_1$ and $\tilde{t}_2$ are the mass eigenstates of the renormalized mass matrix. Accordingly, we can identify $Z_{m_{11}}$ and $Z_{m_{22}}$ with the $\overline{\rm DR}$ renormalization constants $Z_{m_{\tilde{t}_1}}$ and $Z_{m_{\tilde{t}_2}}$ defined through

$$(m_{\tilde{t}_i}^2)^{(0)} = m_{\tilde{t}_i}^2 Z_{m_{\tilde{t}_i}} , \quad i = 1, 2 . \tag{30}$$

In the $\overline{\rm DR}$ scheme the wave function renormalization constants are independent of the masses, so we can evaluate them solving Eqs. (29) for $m_{\tilde{t}_1} = m_{\tilde{t}_2} = 0$. In addition, we can exploit the symmetry of the matrix $\mathcal{Z}_{\tilde{t}}^{1/2}$ and reparametrize it in terms of the common

wave-function renormalization constant of the fields $\tilde{t}_1$ and $\tilde{t}_2$ and the counterterm of the mixing angle, as follows

$$\mathcal{Z}_{\tilde{t}}^{1/2} \equiv \tilde{Z}_2^{1/2} \begin{pmatrix} \cos\delta\theta_t & \sin\delta\theta_t \\ -\sin\delta\theta_t & \cos\delta\theta_t \end{pmatrix} . \tag{31}$$

We solve Eqs. (29) iteratively by inserting the perturbative expansion of all quantities,

$$\begin{aligned} Z &= 1 + \frac{\alpha_s}{\pi}\delta Z^{(1)} + \left(\frac{\alpha_s}{\pi}\right)^2 \delta Z^{(2)} + \mathcal{O}(\alpha_s^3)\,, \\ \delta\theta_t &= \frac{\alpha_s}{\pi}\delta\theta_t^{(1)} + \left(\frac{\alpha_s}{\pi}\right)^2 \delta\theta_t^{(2)} + \mathcal{O}(\alpha_s^3)\,, \\ \Sigma_{ij} &= \frac{\alpha_s}{\pi}\Sigma_{ij}^{(1)} + \left(\frac{\alpha_s}{\pi}\right)^2 \Sigma_{ij}^{(2)} + \mathcal{O}(\alpha_s^3)\,, \quad i,j = 1,2\,, \end{aligned} \tag{32}$$

and take into account the reparametrization of Eq. (31). At one-loop order we get

$$\begin{aligned} \left[\Sigma_{ii}^{(1)} - m_{\tilde{t}_i}^2(\delta Z_2^{(1)} + \delta Z_{m_{\tilde{t}_i}}^{(1)}) + p^2\delta Z_2^{(1)}\right]\Big|_{\rm pp} &= 0\,, \quad i = 1,2\,, \\ \left[\Sigma_{12}^{(1)} - \delta\theta_t^{(1)}(m_{\tilde{t}_1}^2 - m_{\tilde{t}_2}^2)\right]\Big|_{\rm pp} &= 0\,. \end{aligned} \tag{33}$$

In a first step we solve the first equations with $m_{\tilde{t}_1} = m_{\tilde{t}_2} = 0$ to obtain

$$\delta Z_2^{(1)} = -\frac{1}{p^2}\Sigma_{ii}^{(1)}(p)\Big|_{\rm pp}\,, \quad i = 1 \text{ or } i = 2\,. \tag{34}$$

Afterwards, we determine $\delta Z_{m_{\tilde{t}_i}}^{(1)}$ such that the equations are fulfilled also for finite $m_{\tilde{t}_i}$. The renormalization conditions for $S_{12}^{-1}$ and $S_{21}^{-1}$ in Eq. (29) provide an expression for $\delta\theta_t^{(1)}$:

$$\delta\theta_t^{(1)} = \frac{\Sigma_{12}^{(1)}}{m_{\tilde{t}_1}^2 - m_{\tilde{t}_2}^2}\Big|_{\rm pp}\,. \tag{35}$$

Similarly, at two-loop order we have

$$\begin{aligned} &\Big[\Sigma_{ii}^{(2)} + \Sigma_{ii}^{(1)}\delta Z_2^{(1)} - m_{\tilde{t}_i}^2(\delta Z_2^{(2)} + \delta Z_2^{(1)}\delta Z_{m_{\tilde{t}_i}}^{(1)} + \delta Z_{m_{\tilde{t}_i}}^{(2)}) \\ &+(-1)^{i+1}\delta\theta_t^{(1)}[-2\Sigma_{12}^{(1)} + \delta\theta_t^{(1)}(m_{\tilde{t}_1}^2 - m_{\tilde{t}_2}^2)] + p^2\delta Z_2^{(2)}\Big]\Big|_{\rm pp} = 0 \quad (i = 1,2)\,, \\ &\Big[\Sigma_{12}^{(2)} + \Sigma_{12}^{(1)}\delta Z_2^{(1)} + \delta\theta_t^{(1)}(\Sigma_{11}^{(1)} - \Sigma_{22}^{(1)} - m_{\tilde{t}_1}^2\delta Z_{m_{\tilde{t}_i}}^{(1)} + m_{\tilde{t}_2}^2\delta Z_{m_{\tilde{t}_2}}^{(1)}) \\ &\qquad -(m_{\tilde{t}_1}^2 - m_{\tilde{t}_2}^2)(\delta\theta_t^{(2)} + \delta\theta_t^{(1)}\delta Z_2^{(1)})\Big]\Big|_{\rm pp} = 0\,. \end{aligned} \tag{36}$$

In the following we list the results for the squark mass counterterms and the mixing angle, however, we refrain from providing explicit results for $\delta Z_2^{(1)}$ and $\delta Z_2^{(2)}$, as we do not need them for the actual computation.

Our results for the renormalization constant of the top squark mass $m_{\tilde{t}_1}$ read

$$
\begin{aligned}
m^2_{\tilde{t}_1}\delta Z^{(1)}_{m_{\tilde{t}_1}} &= C_F\left(-m^2_{\tilde{g}} - m^2_t + m_{\tilde{g}} m_t S_t + \frac{m^2_{\tilde{t}_2} - m^2_{\tilde{t}_1}}{4} S_t^2\right)\frac{1}{\epsilon}\,,\\
m^2_{\tilde{t}_1}\delta Z^{(2)}_{m_{\tilde{t}_1}} &= \left\{C_F^2\left[\frac{C_t^2 m^2_{\tilde{g}} m^2_t}{m^2_{\tilde{t}_1} - m^2_{\tilde{t}_2}} + \frac{(1+C_t^2)S_t^2(m^2_{\tilde{t}_1} - m^2_{\tilde{t}_2}) + 8m^2_t}{16} - \frac{(1+C_t^2)m_{\tilde{g}} m_t S_t}{2}\right]\right.\\
&\quad + C_A C_F\left[\frac{9m^2_{\tilde{g}}}{8} + 3\frac{S_t^2(m^2_{\tilde{t}_1} - m^2_{\tilde{t}_2}) + 4m^2_t}{32} - \frac{3m_{\tilde{g}} m_t S_t}{4}\right]\\
&\quad \left. + C_F N_f T_F\left[\frac{-3m^2_{\tilde{g}}}{4} - \frac{S_t^2(m^2_{\tilde{t}_1} - m^2_{\tilde{t}_2}) + 4m^2_t}{16} + \frac{m_{\tilde{g}} m_t S_t}{2}\right]\right\}\frac{1}{\epsilon^2}\\
&\quad + \left\{C_F^2\left[\frac{3m^2_{\tilde{g}}}{4} + \frac{S_t^2(m^2_{\tilde{t}_1} - m^2_{\tilde{t}_2}) + 4m^2_t}{16} - \frac{m_{\tilde{g}} m_t S_t}{2}\right]\right.\\
&\quad + C_A C_F\left[\frac{-11m^2_{\tilde{g}}}{8} - 3\frac{S_t^2(m^2_{\tilde{t}_1} - m^2_{\tilde{t}_2}) + 4m^2_t}{32} + \frac{3m_{\tilde{g}} m_t S_t}{4}\right]\\
&\quad + C_F N_q T_F\left[\frac{3m^2_{\tilde{g}}}{4} + \frac{S_t^2(m^2_{\tilde{t}_1} - m^2_{\tilde{t}_2}) + 8m^2_{\tilde{q}} + 4m^2_t}{16} - \frac{m_{\tilde{g}} m_t S_t}{2}\right]\\
&\quad \left. + C_F N_t T_F\left[\frac{3m^2_{\tilde{g}}}{4} + \frac{S_t^2(m^2_{\tilde{t}_1} - m^2_{\tilde{t}_2}) + 4m^2_{\tilde{t}_1} + 4m^2_{\tilde{t}_2} - 4m^2_t}{16} - \frac{m_{\tilde{g}} m_t S_t}{2}\right]\right\}\frac{1}{\epsilon}\\
&\quad + M^2_\varepsilon\left(-C_A C_F\frac{3}{8} + C_F N_f T_F\frac{1}{4}\right)\frac{1}{\epsilon}\,,
\end{aligned}
\tag{37}
$$

where we have introduced the abbreviations $N_f = N_t + N_q$, $S_t = \sin 2\theta_t$ and $C_t = \cos 2\theta_t$. $N_q$ denotes the number of light quark flavours and takes in our case the value $N_q = 5$. $N_t = 1$ has been introduced for convenience. Furthermore $M_\varepsilon$ denotes the on-shell renormalized $\varepsilon$-scalar mass. The corresponding results for $m_{\tilde{t}_2}$ can be derived from Eq. (37) by interchanging $m_{\tilde{t}_1}$ and $m_{\tilde{t}_2}$ and changing the sign of $\theta_t$.

We have employed two different approaches for the renormalization of the $\varepsilon$-scalar mass. In one approach we renormalize it on-shell and choose $M_\varepsilon \neq 0$. In order to decouple the unphysical parameter $M_\varepsilon$ from the physical observables, *i.e.* $M_h$ in our case, we modify the top squark masses by a finite counterterm. This renormalization scheme is equivalent to the $\overline{\text{DR}}'$ scheme [53,54]. However, in the original version of the $\overline{\text{DR}}'$ scheme the $\varepsilon$-scalar mass is renormalized minimally, whereas we choose the on-shell scheme. Thus, the finite

counterterms we found differ starting from two-loops from the ones given in Ref. [54] by

$$\begin{aligned}\delta m^2_{\tilde{t}_i} &= M^2_\varepsilon \left(\frac{\alpha_s}{\pi}\right)^2 \left[ -\frac{C_F^2}{4} + C_A C_F \frac{-3 - 4L_{\mu\varepsilon} + L_{\mu\tilde{g}}}{8} \right. \\ &\quad \left. + C_F N_q T_F \frac{1 + L_{\mu\varepsilon}}{4} + C_F N_t T_F \frac{-1 + L_{\mu t}}{4} \right], \quad i = 1, 2\,, \end{aligned} \tag{38}$$

with $L_{\mu x} = \ln(\mu^2/m_x^2)$ and $L_{\mu\varepsilon} = \ln(\mu^2/M_\varepsilon^2)$. In the second approach we set the on-shell $\varepsilon$-scalar mass to zero. Of course, no finite counterterm is needed in this case. The results for $M_h$ obtained employing the two methods are identical, however, the second approach is computationally less involved. Thus for the practical calculation we set the on-shell $\varepsilon$-scalar mass to zero.
Let us mention that strictly speaking our renormalization coincides neither $\overline{\rm DR}$ nor $\overline{\rm DR}'$ due to the different treatment of the $\varepsilon$-scalar mass. Nevertheless we use the nomenclature "$\overline{\rm DR}$ scheme".

Finally, for the mixing angle we have

$$\begin{aligned}(m^2_{\tilde{t}_1} - m^2_{\tilde{t}_2})\delta\theta_t^{(1)} &= C_F C_t \left( m_{\tilde{g}} m_t - \frac{S_t(m^2_{\tilde{t}_1} - m^2_{\tilde{t}_2})}{4} \right) \frac{1}{\epsilon}\,, \\ (m^2_{\tilde{t}_1} - m^2_{\tilde{t}_2})\delta\theta_t^{(2)} &= \left\{ C_F^2 C_t \left[ (S_t^2 - C_t^2) \left( \frac{m_{\tilde{g}} m_t}{2} - \frac{S_t(m^2_{\tilde{t}_1} - m^2_{\tilde{t}_2})}{16} \right) - \frac{2 S_t m^2_{\tilde{g}} m_t^2}{m^2_{\tilde{t}_1} - m^2_{\tilde{t}_2}} \right] \right. \\ &\quad + C_F C_A C_t \left[ \frac{-3 m_{\tilde{g}} m_t}{4} + \frac{3 S_t(m^2_{\tilde{t}_1} - m^2_{\tilde{t}_2})}{32} \right] + C_F N_f T_F C_t \left[ \frac{m_{\tilde{g}} m_t}{2} - \frac{S_t(m^2_{\tilde{t}_1} - m^2_{\tilde{t}_2})}{16} \right] \Big\} \frac{1}{\epsilon^2} \\ &\quad + \left\{ C_F^2 C_t \left[ -\frac{m_{\tilde{g}} m_t}{2} + \frac{S_t(m^2_{\tilde{t}_1} - m^2_{\tilde{t}_2})}{16} \right] + C_F C_A C_t \left[ \frac{3 m_{\tilde{g}} m_t}{4} - \frac{3 S_t(m^2_{\tilde{t}_1} - m^2_{\tilde{t}_2})}{32} \right] \right. \\ &\quad \left. + C_F N_f T_F C_t \left[ -\frac{m_{\tilde{g}} m_t}{2} + \frac{S_t(m^2_{\tilde{t}_1} - m^2_{\tilde{t}_2})}{16} \right] \right\} \frac{1}{\epsilon}\,. \end{aligned} \tag{39}$$

The two-loop counterterms given in Eqs. (37) and (39) can also be derived from the more general results available in the literature [55–57].

The on-shell renormalization constant of the $\varepsilon$-scalar mass to one-loop order is given by

$$(M^2_\varepsilon)^{(0)} = M^2_\varepsilon Z_{M^2_\varepsilon}\,, \quad Z_{M^2_\varepsilon} = 1 + \frac{\alpha_s}{\pi} \delta Z^{(1)}_{M^2_\varepsilon} + \mathcal{O}(\alpha_s^2)\,, \tag{40}$$

where

$$
\begin{aligned}
-M_\varepsilon^2 \delta Z_{M_\varepsilon^2}^{(1)} &= \left[\frac{C_A}{4}(3M_\varepsilon^2 + 2m_{\tilde{g}}^2) - \frac{N_q T_F}{2}(M_\varepsilon^2 + 2m_{\tilde{q}}^2) - \frac{N_t T_F}{2}(M_\varepsilon^2 + m_{\tilde{t}_1}^2 + m_{\tilde{t}_2}^2 - 2m_t^2)\right]\frac{1}{\epsilon} \\
&+ \frac{C_A}{4}[(6 + 4L_{\mu\varepsilon} - L_{\mu\tilde{g}})M_\varepsilon^2 + 2(1 + L_{\mu\tilde{g}})m_{\tilde{g}}^2] \\
&- \frac{N_q T_F}{2}[(2 + L_{\mu\varepsilon})M_\varepsilon^2 + 2(1 + L_{\mu\tilde{q}})m_{\tilde{q}}^2] \\
&- \frac{N_t T_F}{2}[L_{\mu t} M_\varepsilon^2 + (1 + L_{\mu\tilde{t}_1})m_{\tilde{t}_1}^2 + (1 + L_{\mu\tilde{t}_2})m_{\tilde{t}_2}^2 - 2(1 + L_{\mu t})m_t^2]\,. \qquad (41)
\end{aligned}
$$

The two-loop renormalization constant for the top quark mass in the $\overline{\rm DR}$ scheme is known for long time [58, 59]. For the convenience of the reader we quote the results which are given by

$$
m_t^{(0)} = m_t Z_{m_t}\,, \quad \text{with} \quad Z_{m_t} = 1 + \frac{\alpha_s}{\pi}\delta Z_{m_t}^{(1)} + \left(\frac{\alpha_s}{\pi}\right)^2 \delta Z_{m_t}^{(2)} + \mathcal{O}(\alpha_s^3)\,, \qquad (42)
$$

and

$$
\begin{aligned}
\delta Z_{m_t}^{(1)} &= -C_F \frac{1}{2\epsilon}\,, \\
\delta Z_{m_t}^{(2)} &= \left(\frac{1}{8}C_F^2 + \frac{3}{16}C_A C_F - \frac{1}{8}C_F N_f T_F\right)\frac{1}{\epsilon^2} \\
&+ \left(\frac{1}{8}C_F^2 - \frac{3}{16}C_A C_F + \frac{1}{8}C_F N_f T_F\right)\frac{1}{\epsilon}\,. \qquad (43)
\end{aligned}
$$

The same is true for the one-loop gluino mass counterterm [58, 59] defined through

$$
m_{\tilde{g}}^{(0)} = m_{\tilde{g}} Z_{m_{\tilde{g}}}\,, \quad \text{with} \quad Z_{m_{\tilde{g}}} = 1 + \frac{\alpha_s}{\pi}\delta Z_{m_{\tilde{g}}}^{(1)} + \mathcal{O}(\alpha_s^2)\,, \qquad (44)
$$

with

$$
\delta Z_{m_{\tilde{g}}}^{(1)} = \left(-\frac{3}{4}C_A + \frac{1}{2}N_f T_F\right)\frac{1}{\epsilon}\,. \qquad (45)
$$

# Appendix B: Modification of the $\overline{\rm DR}$ scheme: $\overline{\rm MDR}$

As discussed in Section 3, the renormalization constants of the top squarks have mass dimension two. Thus, for some hierarchies considered in this paper parametrically (and numerically) large corrections might appear which are absent in the on-shell scheme. In order to cure this problem we introduce additional finite corrections in the corresponding renormalization constants which ensure that the renormalized result for the Higgs boson mass is free of these potentially dangerous contributions.

In the following we provide analytic expressions for the finite shifts introduced in the top squark mass counterterms as compared to the $\overline{\rm DR}$ scheme. According to the discussion in Section 3, one can distinguish three cases for the mass hierarchies.

Case (i): $m_{\tilde{q}} \gg m_{\tilde{t}_i}$, $(i = 1, 2)$

$$\left(\frac{m_{\tilde{t}_i}^{\overline{\rm MDR}}}{m_{\tilde{t}_i}}\right)^2 = 1 - \left(\frac{\alpha_s}{\pi}\right)^2 C_F N_q T_F \frac{m_{\tilde{q}}^2}{m_{\tilde{t}_i}^2}\left(-\frac{1}{2} + L_{\mu\tilde{q}} + \zeta(2)\right). \tag{46}$$

The label $N_q = 5$ has been introduced for convenience and for the logarithms the abbreviation $L_{\mu\tilde{q}} = \ln(\mu^2/m_{\tilde{q}}^2)$ has been introduced.

Case (ii): $m_{\tilde{t}_2} \gg m_{\tilde{t}_1}$

$$\left(\frac{m_{\tilde{t}_1}^{\overline{\rm MDR}}}{m_{\tilde{t}_1}}\right)^2 = 1 - \left(\frac{\alpha_s}{\pi}\right)^2 C_F T_F \frac{m_{\tilde{t}_2}^2}{m_{\tilde{t}_1}^2}\left(-\frac{1}{4} + \frac{1}{2}L_{\mu\tilde{t}_2} + \frac{1}{2}\zeta(2)\right). \tag{47}$$

In this equation we have $L_{\mu\tilde{t}_2} = \ln(\mu^2/m_{\tilde{t}_2}^2)$.

Case (iii): $m_{\tilde{g}} \gg m_{\tilde{t}_i}$, $(i = 1, 2)$ and $m_{\tilde{q}} \gg m_{\tilde{g}}$

$$\begin{aligned}
\left(\frac{m_{\tilde{t}_i}^{\overline{\rm MDR}}}{m_{\tilde{t}_i}}\right)^2 &= 1 + \frac{\alpha_s}{\pi}C_F\left[1 + L_{\mu\tilde{g}}\right]\frac{m_{\tilde{g}}^2}{m_{\tilde{t}_i}^2} + \left(\frac{\alpha_s}{\pi}\right)^2\left\{C_F^2\left[-\frac{11}{4} - \frac{3}{2}L_{\mu\tilde{g}} + \zeta(2)\right]\frac{m_{\tilde{g}}^2}{m_{\tilde{t}_i}^2}\right. \\
&+ C_A C_F\left[\frac{21}{8} + \frac{7}{2}L_{\mu\tilde{g}} + \frac{9}{8}L_{\mu\tilde{g}}^2 - \frac{1}{4}\zeta(2)\right]\frac{m_{\tilde{g}}^2}{m_{\tilde{t}_i}^2} \\
&+ C_F N_t T_F\left[-\left(2 + 2L_{\mu\tilde{g}} + \frac{3}{4}L_{\mu\tilde{g}}^2\right)\frac{m_{\tilde{g}}^2}{m_{\tilde{t}_i}^2} + (1 - 2\zeta(2))\frac{m_{\tilde{g}}(m_{\tilde{g}} - m_{\tilde{t}_2})}{m_{\tilde{t}_i}^2}\right] \\
&+ C_F N_q T_F\left[\left(-\frac{5}{8} - \frac{3}{4}L_{\mu\tilde{g}} - \frac{5}{4}L_{\mu\tilde{q}} - \frac{3}{2}L_{\mu\tilde{g}}L_{\mu\tilde{q}} + \frac{3}{4}L_{\mu\tilde{q}}^2 + \frac{3}{2}\zeta(2)\right)\frac{m_{\tilde{g}}^2}{m_{\tilde{t}_i}^2}\right. \\
&+ \left.\left.\left(-\frac{43}{36} - \frac{5}{6}L_{\tilde{q}\tilde{g}}\right)\frac{m_{\tilde{g}}^4}{m_{\tilde{q}}^2 m_{\tilde{t}_i}^2} + \left(-\frac{67}{288} - \frac{7}{24}L_{\tilde{q}\tilde{g}}\right)\frac{m_{\tilde{g}}^6}{m_{\tilde{q}}^4 m_{\tilde{t}_i}^2}\right]\right\}.
\end{aligned} \tag{48}$$

Here $N_t = 1$, $L_{\mu\tilde{g}} = \ln(\mu^2/m_{\tilde{g}}^2)$ and $L_{\tilde{q}\tilde{g}} = \ln(m_{\tilde{q}}^2/m_{\tilde{g}}^2)$.

Case (iv): $m_{\tilde{g}} \gg m_{\tilde{t}_i}$, $(i = 1, 2)$ and $m_{\tilde{q}} \approx m_{\tilde{g}}$

$$\begin{aligned}
\left(\frac{m_{\tilde{t}_i}^{\overline{\rm MDR}}}{m_{\tilde{t}_i}}\right)^2 &= 1 + \frac{\alpha_s}{\pi} C_F \left[1 + L_{\mu\tilde{g}}\right] \frac{m_{\tilde{g}}^2}{m_{\tilde{t}_i}^2} + \left(\frac{\alpha_s}{\pi}\right)^2 \left\{ C_F^2 \left[ -\frac{11}{4} - \frac{3}{2} L_{\mu\tilde{g}} + \zeta(2) \right] \frac{m_{\tilde{g}}^2}{m_{\tilde{t}_i}^2} \right. \\
&+ C_A C_F \left[ \frac{21}{8} + \frac{7}{2} L_{\mu\tilde{g}} + \frac{9}{8} L_{\mu\tilde{g}}^2 - \frac{1}{4}\zeta(2) \right] \frac{m_{\tilde{g}}^2}{m_{\tilde{t}_i}^2} \\
&+ C_F N_t T_F \left[ -\left(2 + 2L_{\mu\tilde{g}} + \frac{3}{4} L_{\mu\tilde{g}}^2\right) \frac{m_{\tilde{g}}^2}{m_{\tilde{t}_i}^2} + (1 - 2\zeta(2)) \frac{m_{\tilde{g}}(m_{\tilde{g}} - m_{\tilde{t}_2})}{m_{\tilde{t}_i}^2} \right] \\
&+ C_F N_q T_F \left[ \left( -\frac{3}{4} L_{\mu\tilde{g}} - \frac{5}{4} L_{\mu\tilde{q}} - \frac{3}{2} L_{\mu\tilde{g}} L_{\mu\tilde{q}} + \frac{3}{4} L_{\mu\tilde{q}}^2 + \frac{3}{2}\zeta(2) \right) \frac{m_{\tilde{g}}^2}{m_{\tilde{t}_i}^2} \right. \\
&- \left. \left. 4\zeta(2) \frac{m_{\tilde{g}}(m_{\tilde{g}} - m_{\tilde{t}_2})}{m_{\tilde{t}_i}^2} - \frac{9}{4} \frac{m_{\tilde{q}}^2}{m_{\tilde{t}_i}^2} \right] \right\}. \qquad (49)
\end{aligned}$$

All the masses on the r.h.s. of the Eqs. (46), (47), (48) and (49) are $\overline{\rm DR}$ masses. Cases (i) and (ii) are applied for all hierarchies whereas cases (iii) and (iv) are only used for (h6) and (h6b), respectively. Let us also mention that the above formulae are valid for the case $M_\varepsilon = 0$.

# Appendix C: SPS scenarios

In the following table we list the input values for the MSUGRA SPS scenarios as defined in Refs. [19, 20]. All masses are given in GeV and $\mathrm{sign}(\mu_{\rm SUSY}) = 1$.

| | Points | | | | Slopes | |
|---|---|---|---|---|---|---|
| | $m_0$ | $m_{1/2}$ | $A_0$ | $\tan\beta$ | $m_0$ | $A_0$ |
| SPS1a′ | 70 | 250 | −300 | 10 | – | – |
| SPS1a | 100 | 250 | −100 | 10 | $0.4m_{1/2}$ | $-0.4m_{1/2}$ |
| SPS1b | 200 | 400 | 0 | 30 | – | – |
| SPS2 | 1450 | 300 | 0 | 10 | $2m_{1/2} + 850$ | 0 |
| SPS3 | 90 | 400 | 0 | 10 | $0.25m_{1/2} - 10$ | 0 |
| SPS4 | 400 | 300 | 0 | 50 | – | – |
| SPS5 | 150 | 300 | −1000 | 5 | – | – |

# References


[1] H. P. Nilles, Phys. Rept. **110** (1984) 1.

[2] H. E. Haber and G. L. Kane, Phys. Rept. **117** (1985) 75.

[3] S. Heinemeyer, W. Hollik and G. Weiglein, Phys. Rept. **425** (2006) 265 [arXiv:hep-ph/0412214].

[4] J. R. Ellis, G. Ridolfi and F. Zwirner, Phys. Lett. B **257** (1991) 83; Phys. Lett. B **262** (1991) 477.

[5] Y. Okada, M. Yamaguchi and T. Yanagida, Prog. Theor. Phys. **85** (1991) 1.

[6] H. E. Haber and R. Hempfling, Phys. Rev. Lett. **66** (1991) 1815.

[7] S. Heinemeyer, Int. J. Mod. Phys. A **21** (2006) 2659 [arXiv:hep-ph/0407244].

[8] B. C. Allanach, A. Djouadi, J. L. Kneur, W. Porod and P. Slavich, JHEP **0409** (2004) 044 [arXiv:hep-ph/0406166].

[9] M. Frank, T. Hahn, S. Heinemeyer, W. Hollik, H. Rzehak and G. Weiglein, JHEP **0702** (2007) 047 [arXiv:hep-ph/0611326].

[10] S. P. Martin, Phys. Rev. D **67** (2003) 095012 [arXiv:hep-ph/0211366].

[11] S. P. Martin, Phys. Rev. D **75** (2007) 055005 [arXiv:hep-ph/0701051].

[12] R. V. Harlander, P. Kant, L. Mihaila and M. Steinhauser, Phys. Rev. Lett. **100** (2008) 191602 [Phys. Rev. Lett. **101** (2008) 039901] [arXiv:0803.0672 [hep-ph]].

[13] S. Heinemeyer, W. Hollik and G. Weiglein, Comput. Phys. Commun. **124** (2000) 76 [arXiv:hep-ph/9812320].

[14] G. Degrassi, S. Heinemeyer, W. Hollik, P. Slavich and G. Weiglein, Eur. Phys. J. C **28** (2003) 133 [arXiv:hep-ph/0212020].

[15] S. Heinemeyer, W. Hollik and G. Weiglein, Eur. Phys. J. C **9** (1999) 343 [arXiv:hep-ph/9812472];

[16] T. Hahn, S. Heinemeyer, W. Hollik, H. Rzehak and G. Weiglein, Comput. Phys. Commun. **180** (2009) 1426.

[17] J. S. Lee, A. Pilaftsis, M. S. Carena, S. Y. Choi, M. Drees, J. R. Ellis and C. E. M. Wagner, Comput. Phys. Commun. **156** (2004) 283 [arXiv:hep-ph/0307377].

[18] J. S. Lee, M. Carena, J. Ellis, A. Pilaftsis and C. E. M. Wagner, Comput. Phys. Commun. **180** (2009) 312 [arXiv:0712.2360 [hep-ph]].

[19] B. C. Allanach *et al.*, in *Proc. of the APS/DPF/DPB Summer Study on the Future of Particle Physics (Snowmass 2001)* ed. N. Graf, Eur. Phys. J. C **25** (2002) 113 [arXiv:hep-ph/0202233].

[20] J. A. Aguilar-Saavedra *et al.*, Eur. Phys. J. C **46** (2006) 43 [arXiv:hep-ph/0511344].

[21] http://www-ttp.particle.uni-karlsruhe.de/Progdata/ttp10/ttp10-23/.

[22] http://www.feynhiggs.de/.

[23] P. H. Chankowski, S. Pokorski and J. Rosiek, Phys. Lett. B **274** (1992) 191.

[24] A. Brignole, Phys. Lett. B **281**, 284 (1992).

[25] A. Dabelstein, Z. Phys. C **67**, 495 (1995) [arXiv:hep-ph/9409375].

[26] G. Degrassi, P. Slavich and F. Zwirner, Nucl. Phys. B **611** (2001) 403 [arXiv:hep-ph/0105096].

[27] B. C. Allanach, Comput. Phys. Commun. **143** (2002) 305 [arXiv:hep-ph/0104145].

[28] Y. Schröder and M. Steinhauser, Phys. Lett. B **622** (2005) 124 [arXiv:hep-ph/0504055].

[29] K. G. Chetyrkin, M. Faisst, J. H. Kühn, P. Maierhöfer and C. Sturm, Phys. Rev. Lett. **97** (2006) 102003 [arXiv:hep-ph/0605201].

[30] R. Boughezal and M. Czakon, Nucl. Phys. B **755** (2006) 221 [arXiv:hep-ph/0606232].

[31] P. Nogueira, J. Comput. Phys. **105** (1993) 279.

[32] R. V. Harlander, L. Mihaila and M. Steinhauser, Eur. Phys. J. C **63** (2009) 383 [arXiv:0905.4807 [hep-ph]].

[33] A. Denner, H. Eck, O. Hahn and J. Küblbeck, Nucl. Phys. B **387** (1992) 467.

[34] J. A. M. Vermaseren, [arXiv:math-ph/0010025].

[35] R. Harlander, T. Seidensticker and M. Steinhauser, Phys. Lett. B **426** (1998) 125, [arXiv:hep-ph/9712228].

[36] T. Seidensticker, [arXiv:hep-ph/9905298].

[37] V. A. Smirnov, "Applied asymptotic expansions in momenta and masses," Springer Tracts Mod. Phys. **177** (2002) 1.

[38] M. Steinhauser, Comput. Phys. Commun. **134** (2001) 335, [arXiv:hep-ph/0009029].

[39] P. Skands *et al.*, JHEP **0407** (2004) 036 [arXiv:hep-ph/0311123].

[40] A. Djouadi, J. L. Kneur and G. Moultaka, Comput. Phys. Commun. **176** (2007) 426 [arXiv:hep-ph/0211331].

[41] W. Porod, Comput. Phys. Commun. **153** (2003) 275 [arXiv:hep-ph/0301101].

[42] S. P. Martin, Phys. Rev. D **72**, 096008 (2005) [arXiv:hep-ph/0509115].

[43] S. P. Martin and D. G. Robertson, Comput. Phys. Commun. **174**, 133 (2006) [arXiv:hep-ph/0501132].

[44] Tevatron Electroweak Working Group and CDF Collaboration and D0 Collaboration, [arXiv:0903.2503 [hep-ex]].

[45] R. Harlander, L. Mihaila and M. Steinhauser, Phys. Rev. D **72** (2005) 095009 [arXiv:hep-ph/0509048].

[46] R. V. Harlander, L. Mihaila and M. Steinhauser, Phys. Rev. D **76**, 055002 (2007) [arXiv:0706.2953 [hep-ph]].

[47] A. Bauer, L. Mihaila and J. Salomon, JHEP **0902** (2009) 037 [arXiv:0810.5101 [hep-ph]].

[48] S. Bethke, Eur. Phys. J. C **64** (2009) 689 [arXiv:0908.1135 [hep-ph]].

[49] T. van Ritbergen, J. A. M. Vermaseren and S. A. Larin, Phys. Lett. B **400** (1997) 379 [arXiv:hep-ph/9701390].

[50] M. Czakon, Nucl. Phys. B **710** (2005) 485 [arXiv:hep-ph/0411261].

[51] I. Jack, D. R. T. Jones and C. G. North, Phys. Lett. B **386** (1996) 138 [arXiv:hep-ph/9606323].

[52] M. S. Carena, S. Heinemeyer, C. E. M. Wagner and G. Weiglein, Eur. Phys. J. C **26** (2003) 601 [arXiv:hep-ph/0202167].

[53] I. Jack, D. R. T. Jones, S. P. Martin, M. T. Vaughn and Y. Yamada, Phys. Rev. D **50** (1994) 5481 [arXiv:hep-ph/9407291].

[54] S. P. Martin, Phys. Rev. D **65** (2002) 116003 [arXiv:hep-ph/0111209].

[55] I. Jack and D. R. T. Jones, Phys. Lett. B **333** (1994) 372 [arXiv:hep-ph/9405233].

[56] Y. Yamada, Phys. Rev. D **50** (1994) 3537 [arXiv:hep-ph/9401241].

[57] S. P. Martin and M. T. Vaughn, Phys. Rev. D **50** (1994) 2282 [Erratum-ibid. D **78** (2008) 039903] [arXiv:hep-ph/9311340].

[58] D. R. T. Jones and L. Mezincescu, Phys. Lett. B **136** (1984) 242; Ibid. **138** (1984) 293.

[59] A. J. Parkes and P. C. West, Nucl. Phys. B **256** (1985) 340.